Significant role of biomass burning in heavy haze formation in Nanjing, a megacity in China: Molecular-level insights from intensive $PM_{2.5}$ sampling on winter hazy days

Mingjie Kang[1,2], Mengying Bao[1,2,3], Wenhuai Song[1,2], Aduburexiati Abulimiti[1,2], Changliu Wu[1,2], Fang Cao[1,2], Sönke Szidat[4], Yanlin Zhang[1,2]

[1] School of Ecology and Applied Meteorology, Nanjing University of Information Science and Technology. Nanjing 210044, China.

[2] Atmospheric Environment Center, Joint Laboratory for International Cooperation on Climate and Environmental Change, Ministry of Education, Nanjing University of Information Science and Technology. Nanjing 210044, China.

[3] Huzhou Meteorological Administration, Huzhou, 313000, China

[4] Department of Chemistry, Biochemistry and Pharmaceutical Sciences & Oeschger Centre for Climate Change Research, University of Bern, Bern, 3012, Switzerland

Correspondence to: Yanlin Zhang (zhangyanlin@nuist.edu.cn; dryanlinzhang@outlook.com)

Abstract. Reports on the molecular-level characterization of primary and secondary constituents in $PM_{2.5}$ at high temporal resolution, particularly during haze events, are still limited. This study employed comprehensive analytical methods to examine the molecular composition and source contributions of $PM_{2.5}$, with samples collected approximately every two hours during hazy winter days. Results show that organic matter was the predominant species, followed by nitrate (NO_3^-). Radiocarbon analysis of carbonaceous fractions reveals that fossil fuels account for 61–82% of water-soluble organic carbon (WSOC), reflecting increased coal combustion for residential cooking and heating, as well as coal-fired industries during colder months. Interestingly, the contribution of non-fossil sources to WSOC enhanced with worsening haze pollution, coinciding with significantly intensified biomass burning (BB). BB emerged as the largest contributor to organic carbon (OC) in both concentration and proportion, likely due to increased oxidants and aqueous SOA formation from BB-derived gases, especially under polluted conditions with low temperatures and high relative humidity (RH). For secondary sources, naphthalene-derived secondary organic carbon (SOC) contributed more to OC in $PM_{2.5}$ (0.27–2.46%) compared to biogenic SOC (0.05–1.10%), suggesting anthropogenic VOCs greatly contribute to SOC in urban aerosols during winter. Total tracer-based SOC exhibited higher levels on days with elevated temperatures and lower RH due to enhanced photooxidation. In addition to increasing secondary aerosol formation, BB can also enhance emissions from other sources, as evidenced by significant correlations between BB tracers and various other source tracers. These findings highlight the significant role of BB in contributing to heavy winter haze.

1. Introduction

The air quality of China has significantly improved over the past decade due to widespread implementation of emission controls. However, this progress was unexpectedly disrupted by severe air pollution during the COVID-19 lockdown, when anthropogenic emissions dropped dramatically (Huang et al., 2020b; Le et al., 2020; Wang et al., 2020). This highlights the persistent challenge of controlling $PM_{2.5}$ pollution, especially during cold seasons in megacities. Moreover, the emergence of ozone (O_3) pollution in many urban areas complicates the situation. Rising O_3 levels, associated with increased atmospheric oxidation capacity (Kang et al., 2021), lead to more complex air pollution scenarios due to intricate secondary aerosol formations and the combined effects of $PM_{2.5}$ and O_3.

$PM_{2.5}$ affects air visibility, regional and global radiation balance, the hydrological cycle (Kaufman et al., 2002), and both human and ecosystem health (Alexeeff et al., 2023; Chen et al., 2022; Pope et al., 2004; Wang et al., 2022). In response, scientists have conducted numerous studies to analyze aerosol components and emission sources (Cheng et al., 2016; Huang et al., 2014, 2020b, a; Jimenez et al., 2009; Kang et al., 2016, 2018a, b, 2019; Li et al., 2016a; Liu et al., 2014; Sun et al., 2014; Wang et al., 2006; Yang et al., 2024; Zhang et al., 2012, 2018). These studies indicate that $PM_{2.5}$ pollution results from the interplay of primary and secondary sources, encompassing both anthropogenic and biogenic origins. Primary sources include plant emissions, fungal spores, soil dust, fossil fuel combustion, and biomass burning (BB) (Anon, 2002; Fu et al., 2012; Kang et al., 2018b, a; Morris et al., 2011; Pöschl et al., 2010; Simoneit, 2002; Zhang et al., 2015, 2016). Secondary sources primarily involve the homogeneous and heterogeneous reactions of biogenic and anthropogenic precursors (e.g., NO_x, NH_3, SO_2, and VOCs) (Fu et al., 2010; Huang et al., 2014). Many $PM_{2.5}$ species contain origin information and can therefore serve as tracers to identify specific sources.

For example, saccharides, including anhydrosugars, sugars, and sugar alcohols, are important water-soluble organic constituents of aerosols (Simoneit et al., 2004b; Sindelarova et al., 2014). These compounds can act as cloud condensation nucleus and ice nuclei, thus influencing Earth's climate and water supply (Kaufman et al., 2002). Among them, levoglucosan is widely used as a typical tracer for BB (Elias et al., 2001; Li et al., 2021b; Liu et al., 2013). BB has a substantial

impact on the secondary organic aerosols (SOA) budget and climate change (Chen et al., 2017b; Zhang et al., 2024). For instance, substituted phenols from lignin combustion, which also serve as BB tracers, undergo aqueous phase oxidation with photooxidants to form SOA, significantly influencing the evolution of organic aerosols (Zhang et al., 2024). However, the contribution of BB emissions to SOA formation is not yet well understood, leading to inaccurate representation in regional and global atmospheric chemistry models. Sugar alcohols, such as arabitol and mannitol, can be used to assess the contribution of airborne fungal spores to carbonaceous aerosols (Bauer et al., 2008a, b; Fu et al., 2012, 2016). Additionally, primary sugars like glucose are useful markers for plant pollen, fruits, and detritus (Fu et al., 2016; Puxbaum and Tenze-Kunit, 2003).

Secondary organic aerosols (SOA) are also a significant fraction of atmospheric aerosols, formed through the reactions of oxidants (e.g., OH) with both biogenic and anthropogenic VOCs (Claeys et al., 2004; Hallquist et al., 2009; Huang et al., 2014; Mozaffar et al., 2020). Biogenic VOCs, such as isoprene, monoterpenes, and sesquiterpenes, play a crucial role in global SOA formation and atmospheric processes (Claeys et al., 2004; Griffin et al., 1999; Guenther et al., 2006; Pöschl et al., 2010; Sindelarova et al., 2014; Zhang et al., 2007). In contrast, anthropogenic VOCs (e.g., aromatic hydrocarbons) are more prevalent in urban areas where coal combustion, transportation, solvent use and biofuel/biomass burning significantly contribute (Chen et al., 2017b; Ding et al., 2017; Srivastava et al., 2022). Despite their importance, comprehensive characterization of SOA at the molecular level is challenging due to complex formation processes and fluctuating meteorological conditions. The lack of detailed molecular-level information regarding the composition, abundance, and formation mechanisms of SOA at high temporal resolution introduces uncertainties in modeling and forecasting of air pollutants (Zhang et al., 2022, 2023). As a result, accurately simulating SOA with chemical transport models becomes increasingly difficult.

In addition to the organic species mentioned above, secondary inorganic aerosols (SIA), which include sulfate (SO_4^{2-}), nitrate (NO_3^-), and ammonium (NH_4^+), also constitute a significant portion of fine aerosols, particularly on heavily polluted days (Fu et al., 2012; Huang et al., 2014; Lu et al., 2019; Yan et al., 2023). Nitrate and sulfate in $PM_{2.5}$ are primarily formed through

secondary processes and are expected to have substantial regional impacts upon emission, especially in winter. A recent study reported that nitrate made up the largest fraction of $PM_{2.5}$ in China during severe haze events, and reducing NO_x emissions was considered an effective strategy for combating air pollution (Yan et al., 2023). However, this conclusion was called into question by the persistent severe haze during the COVID-19 lockdown, when NO_x emissions significantly declined (Le et al., 2020), suggesting the complexity of $PM_{2.5}$ pollution and the need for further research.

Although previous studies have provided valuable insights into aerosol components, the molecular-level compositions and concentrations of fine particles remain poorly understood due to their high spatial and temporal variability, especially at sub-daily (hourly) levels. One reason for this gap is that aerosol properties can change during transport through dry or wet deposition, in-cloud processes, and atmospheric chemical reactions. Therefore, intensive aerosol sampling at high temporal resolution is essential for accurately quantifying $PM_{2.5}$ components and their source contributions. Most prior studies have focused on comparing hazy and clean days, with few studies examining variations among different hazy days on a sub-daily basis, partly due to the challenges associated with frequent aerosol sampling. However, such molecular-level data at high temporal resolution are crucial for identifying the key factors that control haze formation, which is vital for developing regulatory standards that can adapt to rapid changes in aerosol composition and concentrations over time and place. Furthermore, the impacts of aerosol particles with varying properties (e.g., chemical composition) on climate (Kanakidou et al., 2005; Kawana et al., 2022) remain unclear. Obtaining molecular-level $PM_{2.5}$ data at hourly intervals would greatly enhance our understanding of these issues.

In this study, we systematically unraveled the hourly variation of molecular-level $PM_{2.5}$ components during haze events in Nanjing, a major city in the Yangtze River Delta with active industries and a dense population. Concentrations of key organic and inorganic components, such as BB tracers, sugar and sugar alcohols, oxidation products (e.g., biogenic SOA tracers and aromatic acids), and water-soluble icons, were measured and compared across three different haze pollution levels. Contributions of primary sources to organic carbon (OC) in $PM_{2.5}$ samples, including BB, fungal spores, and plant debris, were estimated. Additionally, we

calculated the contributions of secondary OC formed from biogenic and anthropogenic VOCs to the total OC. Radiocarbon measurements were performed on water-soluble organic carbon (WSOC) to accurately assess the contributions of fossil and non-fossil sources. Molecular-level results on $PM_{2.5}$ components and source contributions at high temporal resolution will help understand haze formation and evolution in megacities.

2. Materials and methods

2.1 Sampling

The sampling site was situated on the rooftop of a building at Nanjing University of Information Science and Technology in Nanjing, China (32.2°N, 118.72°E). A total of 23 $PM_{2.5}$ samples were collected on Prebaked quartz fiber filters (Pallflex) at approximately 2-hour intervals from December 31, 2017, to January 2, 2018. A high-volume air sampler (KC-1000, Qingdao Laoshan Electric Inc., China) was used, operating at a flow rate of 1.05 m^3 min^{-1}. Field blanks were also collected with the pump off during sampling. All samples were stored in darkness at −20°C for later analysis. The entire sampling period was divided into three episodes based on $PM_{2.5}$ levels: > 200 μg m^{-3}, 100–200 μg m^{-3}, and <100 μg m^{-3}, reflecting a transition from heavily polluted to moderately polluted days.

2.2 Measurements of organic molecules

Sugar compounds, including anhydrosugars, sugar alcohols, and sugars, were measured using ion chromatography (Dionex ICS-5000+, ThermoFisher Scientific, USA) after extraction with ultra-pure water (Milli-Q Reference, America). Standard curve establishment and blank corrections were performed during the analysis. Other organic compounds, such as biogenic SOA tracers (isoprene, sesquiterpene, and monoterpene) and other significant organic molecules, were determined using gas chromatography/mass spectrometry (Agilent Technologies; Santa Clara, CA). Average recoveries ranged from 70% to 110%, and repeatability tests showed deviations of less than 15%. All data were corrected with field blanks. Further details on measurements can be found in previous studies (Bao et al., 2023). The total mass concentrations of SOC produced by isoprene (using 2-methylglyceric acid and 2-methyltetrols), α/β-pinene, and β-caryophyllene were estimated using the tracer-based method

by Kleindienst et al. (2007). BB-derived OC and fungal-spore-derived OC were calculated using methods from earlier reports (Bauer et al., 2008a; Fu et al., 2014).

2.3 Measurements of OC, EC, WSOC, and inorganic icons

The elemental and organic carbon content was measured using a Sunset Lab EC/OC Analyzer with the Interagency Monitoring of Protected Visual Environments (IMPROVE) 7-step heating method, which has been shown to provide more accurate measurements for EC and OC (Wu et al., 2020). Details regarding the determination of WSOC can be found in Bao et al. (2022). Water-soluble ions were analyzed using ion chromatography (IC), with further information available in Bao et al. (2023). The detected inorganic icons are listed in Table 1.

2.4 ^{14}C analysis of the carbonaceous fractions

The ^{14}C content of WSOC was determined by extracting WSOC with deionized water and then collecting the extracted solution for ^{14}C measurement using chemical wet oxidation of the eluate (Song et al., 2022). The ^{14}C results are expressed as fractions of measured carbon, calculated as follows ($F^{14}C$):

$$F^{14}C = \frac{(^{14}C/^{12}C)_{sample}}{(^{14}C/^{12}C)_{1950}} \quad (1)$$

Where $(^{14}C/^{12}C)_{1950}$ is the reference isotopic ratio from 1950. The $F^{14}C$ values were then corrected by dividing by the reference value ($f_{nf,ref}$) to remove potential impacts of nuclear bomb tests in the 1950s and 1960s, thereby obtaining the non-fossil fractions of WSOC. More details can be found in the papers by Song et al. (2022) and Zhang et al. (2017).

$$f_{nf} = F^{14}C/f_{nf,ref} \quad (2)$$

2.5 Backward trajectories below 500 m above ground level

Regional transport also significantly influences $PM_{2.5}$ levels (Chang et al., 2019; Chen et al., 2017a). To estimate the impacts of air pollution transport on haze formation, we employed the Hybrid Single-Particle Lagrangian Integrated Trajectory (HYSPLIT) model to compute backward trajectories of air masses arriving at the sampling site (available at https://www.ready.noaa.gov/hypub-bin/trajtype.pl?runtype=archive). MODIS active fire/hotspot products were utilized to evaluate the impact of open BB throughout the

sampling period. The backward trajectory analysis revealed that air masses during the sampling period were significantly influenced by BB, as illustrated in Fig. S1. By comparison, the third episode demonstrated a greater influx of clean ocean air masses (Fig. S1c).

3. Results and discussion

3.1 Inorganic icons

Table 1 presents the concentrations of identified inorganic icons, with Cl^-, NO_3^-, SO_4^{2-}, and NH_4^+ being the major inorganic components throughout the sampling period. The contribution of SIA to total $PM_{2.5}$ far exceeded that of organic matters (OM) during all haze episodes, indicating SIA contributes greatly to the occurrence of heavy haze. As illustrated in Figure 1, NO_3^- was the second dominant species (mean: 20.1–25.6%) in $PM_{2.5}$, following OM, particularly during the heaviest haze event, which aligns with findings from a megacity in Canada (Rivellini et al., 2024). However, these percentages are higher than those reported for other megacities by Huang et al. (2014) (7.1–13.6%), likely due to the spatial and temporal variations in energy mix and meteorological conditions over the years. The predominance of NO_3^- in SIA (30–52%) is in agreement with the study on nitrate aerosols in Beijing, another megacity in China (~ 43%) (Fan et al., 2020). Major sources of NO_3^- include vehicles, coal combustion, natural gas burning, and biomass burning (Fan et al., 2023; Lin et al., 2024; Zhang et al., 2014a). The rising levels of NO_3^- relative to SO_4^{2-} may be associated with recent declines in SO_2 emissions and increases in NH_3 emissions, which allows more HNO_3 to condense into particulate NO_3^- (Shah et al., 2024). This is supported by the strong correlation between NO_3^- and NH_4^+ ($r = 0.98$, $p < 0.01$). The highest concentration of NO_3^- (56.0 ± 4.4 μg m^{-3}) and its contribution (~ 25.6%) occurred during the highest-$PM_{2.5}$ episode, likely linked to high relative humidity (RH) during this time (Fig. S2), which usually comes with high aerosol liquid water content (Bian et al., 2014) and accordingly promotes more heterogeneous reactions of nitrate formation (Lin et al., 2020). On the other hand, cooler temperatures during heavy haze episode favor the partitioning of HNO_3 from the gas phase into the particulate phase. NO_3^- also showed a significant correlation with non-sea-salt SO_4^{2-} (nss-SO_4^{2-}) ($r = 0.92$, $p < 0.01$), calculated by subtracting sea-

salt sulfate from total sulfate using the typical sulfate-to-sodium mass ratio of 0.252 in seawater (Yang et al., 2015), suggesting similar sources or formation pathways (Zhang et al., 2014a). Actually, under polluted conditions with high RH, reactive nitrogen chemistry in aerosol water contributes to SO_4^{2-} formation, where NO_x acts both as a precursor for nitrate and as an important oxidant for sulfate (Cheng et al., 2016). Consequently, NO_x emission reductions have great potential for simultaneously decreasing atmospheric sulfate, nitrate, and even O_3 pollution (Kang et al., 2021; Shah et al., 2024). Interestingly, the three SIA components (NO_3^-, SO_4^{2-}, and NH_4^+) were found to have strong correlations with BB tracers (e.g., levoglucosan and mannosan), with $p < 0.01$ and r values ranging from 0.63 to 0.80. This indicates BB significantly enhances the secondary production of SIA. Given that the precursors of NO_3^- and SO_4^{2-} –NO_x and SO_2–are mainly contributed by fossil fuel combustion (e.g., transportation and industrial activities) in urban areas, these relationships suggest that BB play a substantial role in the secondary transformation of fossil-fuel-derived precursors.

3.2 OC, EC, WSOC, and ^{14}C of WSOC

Similarly, the abundance of EC, OC, WSOC, and WISOC decreased with decreasing $PM_{2.5}$ levels, in line with growing wind speeds. In comparison to other episodes, the first episode, in which $PM_{2.5}$ levels exceeded 200 μg m^{-3}, exhibited relatively high RH, low temperatures, and low wind speeds (Fig. S2), demonstrating that adverse meteorological conditions can boost haze formation. As displayed in Table 1, the mass concentrations of OC and EC were in the range of 8.74–41.1 and 1.26–3.08 μg m^{-3}, respectively. These OC values are similar to previous reports for $PM_{2.5}$ in Nanjing, while EC levels are lower (Li et al., 2015, 2016b), reflecting a reduction in primary emissions due to stricter emission controls in recent years. There is a significant correlation between OC and EC (r = 0.87, $p < 0.01$, Fig. S3), suggesting they share common sources, such as BB, vehicle exhaust, and fossil fuel combustion (Ji et al., 2019). The OC/EC ratio increased with rising $PM_{2.5}$ levels, from an average of 8.7 to 13.3 (Table 1 and Fig. 2), close to those in BB-dominated regions (Boreddy et al., 2018; Zhang et al., 2014b). BB is known to emit a higher fraction of OC than EC (Andreae and Merlet, 2001), so the high OC/EC ratios in this study indicate significant contributions from BB, particularly during heavy haze

events. In addition, the high OC/EC ratios (> 2.0–2.2) suggest the presence of secondary organic aerosol (Li et al., 2016b), likely linked to BB as a significant source of oxidants (Chang et al., 2024) and an important contributor to SOA formation (Li et al., 2024; Lim et al., 2019; Yee et al., 2013).

OC can be divided into water-soluble organic carbon (WSOC), which often comprises BB-derived and aged OC, and water-insoluble organic carbon (WISOC), typically representing primary OC (Zhang et al., 2014b). As shown in Fig. 2, the concentration of WISOC (4.55–25.8 μg m^{-3}) is generally higher than that of WSOC, making WISOC the primary component of OC. WSOC concentration ranged from 3.84 to 18.1 μg m^{-3}, with peak values during the most polluted episode averaging 14.3 ± 2.62 μg m^{-3}, comparable to previously reported winter values of 14.0 μg m^{-3} (Li et al., 2018). The WSOC/OC ratios were relatively higher during more polluted episodes ($PM_{2.5}$ > 100 μg m^{-3}), averaging 0.40 ± 0.06 and 0.43 ± 0.03, respectively (Table 1). Higher WSOC/OC ratios (> 0.4) indicate significant contribution from secondary organic aerosol and aged aerosols (Boreddy et al., 2018; Ram et al., 2010). Given the high RH during the most polluted episode, the aqueous-phase oxidation of anthropogenic and/or biogenic VOCs is likely responsible for more WSOC formation during this time (Youn et al., 2013). In contrast, the lower WSOC/OC ratios (0.35 ± 0.17) in the third episode ($PM_{2.5}$ < 100 μg m^{-3}) suggest rising primary emissions containing large amounts of water-insoluble organics (e.g., lipid compounds), as indicated by higher WISOC/OC ratios (0.65 ± 0.17) during that time. WSOC exhibited a strong correlation with levoglucosan (r = 0.74, p < 0.01), highlighting BB as an important contributor to WSOC. This is further supported by significant correlations between BB tracers and water-soluble organic compounds, such as dicarboxylic acids (see details in the Supplement). Soluble organic gases from BB, such as phenols, can react with oxidants in aerosol liquid water and clouds, significantly contributing to SOA formation. Moreover, this aqueous SOA production greatly increases with rising RH (Zhang et al., 2024). Given the high RH during the most polluted episode, aqueous SOA generation from BB-derived organic gases likely plays a crucial role in heavy haze formation. Aqueous SOA generation from BB emissions was also confirmed by multiple studies (Gilardoni et al., 2016; Li et al., 2021a, 2014; Xiao et al., 2022), emphasizing the importance of BB emissions in atmospheric

oxidation processes. A recent report further indicates that intermediate VOCs from BB make a considerable contribution to SOA formation (Li et al., 2024), underscoring BB's significant role in the secondary formation of atmospheric organic aerosols.

To track the trends in fossil and non-fossil contributions to carbonaceous aerosols throughout haze development, ^{14}C measurements were applied to quantify the sources of WSOC. As presented in Table 1 and Fig. 3, the non-fossil fraction of WSOC was in the range of 18–39% (mean: 26%), indicating that fossil fuel sources were the primary contributors to WSOC on winter hazy days (61–82%, mean: 74%) (Fig. S4). These high fossil contributions align with previous observations in Beijing during haze events in winter (~ 61%) (Zhang et al., 2017) and in spring (~ 54%) (Liu et al., 2016). The variations in ^{14}C levels may reflect differing origins and formation processes of WSOC across regions and seasons. The substantial fossil fuel contribution in this study can be attributable to extensive coal combustion for residential cooking and heating on cold days, as well as industrial activities and traffic emissions near the sampling sites. Interestingly, while fossil fuels predominated, the contribution of non-fossil sources increased with haze intensity, suggesting their significant role in heavy haze formation. A similar trend was noted in northern India, where the non-fossil fraction of organic aerosols was higher during polluted cold periods compared to warmer months (Bhattu et al., 2024). Notably, the highest non-fossil percentages (31% ± 6%) coincided with peak BB contributions during the haziest episode. This is evidenced by the relationship between non-fossil WSOC and BB markers (e.g., syringic acid, $r = 0.68$, $p < 0.01$), indicating that BB was a significant non-fossil source of WSOC and likely a key driver of severe winter haze, despite the substantial fossil fuel contribution at the site. Previous studies also emphasized the role of aqueous-phase photochemical oxidation of organic gases from BB in haze pollution (Xiao et al., 2022; Zhang et al., 2024). This aqueous-phase SOA formation can surpass the conventional semi-volatile SOA pathways, especially under polluted conditions with high RH (Zhang et al., 2024). Additionally, BB-chlorine emissions can enhance oxidation capacity, further promoting secondary aerosol formation (Chang et al., 2024). This study found a positive correlation between Cl^- and levoglucosan ($r = 0.50$, $p < 0.05$), suggesting that BB contributes to Cl^- levels at this site and may influence the atmospheric chemistry in this area.

3.3 Carbonaceous components

Figure 4 displays the average concentrations of carbonaceous species in $PM_{2.5}$ across three air pollution episodes. Saturated diacids (1.66–14.6 μg m^{-3}) were the dominant carbonaceous components, followed by sugars and sugar alcohols (278–4936 ng m^{-3}) and anhydrosugars (79.4–801 ng m^{-3}). The higher concentrations of anhydrosugars during the first episode indicate a significant impact from BB during heavy haze events. In contrast, the elevated levels of sugars and sugar alcohols in the latter two episodes are likely attributed to increased wind speeds, which facilitated the resuspension of biogenic detritus and soil microbes rich in these substances. Biogenic SOA tracers were relatively minor during winter haze but showed higher levels in the second episode, probably due to enhanced photooxidation under elevated temperatures and lower RH. Unsaturated aliphatic diacids and aromatic acids presented a similar trend to biogenic SOA. Additionally, lignin and resin acids–alternative tracers for BB–exhibited higher concentrations during heavy haze events, further underscoring the significance of BB in these conditions. The individual organic species identified in this study are discussed in detail below and in the Supporting Information document.

3.3.1 Biomass burning tracers (anhydrosugars and lignin/resin acids)

Levoglucosan, a specific indicator of BB, is produced through the thermal degradation of cellulose (Simoneit, 2002). The highest concentration of levoglucosan was observed during the highest-$PM_{2.5}$ episode (average: 471 ± 122 ng m^{-3}), highlighting the substantial role of BB in severe haze formation (Fig. S5). These levels exceed those reported in winter in Beijing (average: 361 ng m^{-3}) (Li et al., 2018) and are significantly higher than in the marine aerosols (average: 7.3 ng m^{-3}) (Kang et al., 2018a). Mannosan and galactosan, isomers of levoglucosan, serve as primary tracers for hemicellulose pyrolysis (Simoneit, 2002). During the sampling period, their concentrations remained considerably lower than that of levoglucosan (Figs. S5 and S6). Notably, a significant correlation was found between mannosan and levoglucosan ($r = 0.78$, $p < 0.01$), suggesting they share similar sources at this site.

The ratios of levoglucosan to potassium (L/K^+) can be used to differentiate burnings from different biomass (Urban et al., 2012). Both levoglucosan and K^+ are BB tracers, but this study

found no significant correlation between the two. This is because in urban areas airborne potassium has other important sources, including meat cooking, waste incineration, and the resuspension of surface soil and fertilizers (Simoneit, 2002; Urban et al., 2012). The average L/K^+ ratios for the three episodes were 0.51 ± 0.19, 0.20 ± 0.07, and 0.44 ± 0.33, respectively. The lower ratios observed in the second episode may result from increased wind speeds, which facilitate the resuspension of potassium-rich surface soil and fertilizers (Urban et al., 2012). Additionally, the enhanced chemical degradation of levoglucosan at relatively high temperatures and low RH could further lower the L/K^+ ratios (Li et al., 2021b). Overall, the L/K^+ values in this study (0.06–1.04) agree well with those reported for crop and wood burning (Cheng et al., 2013; Urban et al., 2012), implying a mixed biofuel combustion, as supported by the isomeric ratios of anhydrosugars (Fig. S8).

The levoglucosan-to-OC (L/OC) and levoglucosan-to-EC (L/EC) ratios are widely used to evaluate the contribution of BB to aerosol abundance and potential degradation of levoglucosan (Mochida et al., 2010; Sullivan et al., 2008; Zhang et al., 2008). In this study, the L/OC and L/EC ratios are similar to those observed in December in Beijing (Li et al., 2018) but are higher than those for marine aerosols in winter (Zhu et al., 2015a). Higher L/OC and L/EC ratios generally occurred during heavy haze events (Fig. S7), further proving the greater contribution of BB to heavy haze formation. The overall decline in L/OC and L/EC ratios with decreasing $PM_{2.5}$ levels may indicate reduced BB activities as well as increased levoglucosan degradation.

Lignin and resin acids are also found in smoke aerosols from BB and serve as markers for this process (Simoneit, 2002). In this study, the total lignin and resin acids are found in much lower amounts than anhydrosugars (Fig. 4). A total of three lignin products (4-hydroxybenzoic acid, vanillic acid, and syringic acid) and one resin product (dehydroabietic acid) were measured, with the highest concentrations occurring during the highest-$PM_{2.5}$ episode (46.5 ± 38.0 ng m^{-3}), further demonstrating the significant BB influence on heavy haze. These values are comparable to those in wintertime aerosols in Beijing (47.5 ng m^{-3}) (Li et al., 2018). Among the lignin and resin acids, syringic acid was the most abundant during heavy haze episode (~ 28.0 ng m^{-3}), while dehydroabietic acid was more prevalent in moderate and light haze episodes (~ 14.4 and 17.0 ng m^{-3}, respectively). Dehydroabietic acid and vanillic acid are typical tracers

of conifer (softwood) burning, whereas syringic acid is more associated with hardwood smoke (Simoneit, 2002). The relatively high levels of dehydroabietic and syringic acids observed during the highest-$PM_{2.5}$ episode suggest a significant contribution from mixed wood burning on cold days, when considerable firewood was used for residential cooking and heating in nearby suburbs. Additionally, 4-hydroxybenzoic acid (4-HBA), a major tracer from the pyrolysis of non-woody vegetation such as grass and crop residue, ranged from 0.05 to 9.32 ng m^{-3}. A strong correlation between 4-HBA and vanillic acid ($r = 0.86$, $p < 0.01$) indicates their similar sources, such as mixed biofuel burning.

3.3.2 Primary sugars and sugar alcohols

Primary sugars identified in this study include trehalose and glucose, with concentrations in the range of 86.5–3023 ng m^{-3} and 49.3–551 ng m^{-3}, respectively. Trehalose is particularly abundant in soils, especially in the fine mode ($PM_{2.5}$) (Jia and Fraser, 2011), and can serve as a potential tracer for the resuspension of surface soil and unpaved road dust (Fu et al., 2012). This is supported by the similar trends observed for trehalose and non-sea-salt calcium (nss-Ca^{2+}) in the present study, as nss-Ca^{2+} is an indicator for soil dust, particularly in winter and spring (Virkkula et al., 2006). Trehalose showed a higher average concentration (1057 ± 1112 ng m^{-3}) during the second episode, likely linked to increased wind speeds that facilitated the transport of trehalose from surface soil into the air. Glucose, also abundant in biologically active soils, is considered a marker for fugitive dust from cultivated land (Rogge et al., 2007). In addition, glucose is abundant in various plant tissues as well, such as pollen, fruits, developing leaves, and plant detritus (Graham et al., 2003). Both glucose and trehalose exhibited higher levels during moderate haze events, indicating enhanced primary biogenic sources during that time due to rising temperatures and wind speeds (Zhu et al., 2015b).

Sugar alcohols detected in this study consisted of arabitol, mannitol, and glycerol, with concentrations in the range of 4.59–48.2 ng m^{-3}, 0.47–24.4 ng m^{-3}, and 119–4749 ng m^{-3}, respectively. Glycerol was the most abundant sugar alcohol, consistent with findings from previous studies (Kang et al., 2018b; Li et al., 2018; Ren et al., 2020). Glycerol levels increased as $PM_{2.5}$ concentrations declined (Fig. S9), peaking during the lowest-$PM_{2.5}$ episode (~ 2348 ng m^{-3}). This trend may be attributed to rising local temperatures during moderate and light haze

events, as lower ambient temperatures tend to reduce microbial activities, such as fungal spore release. Conversely, higher concentrations of arabitol and mannitol exist in the highest-$PM_{2.5}$ episode (> 200 μg m^{-3}), coinciding with intensified BB. These sugar alcohols can be emitted not only from natural sources like microbial activities and plant tissues but also significantly through thermal stripping during BB (Simoneit et al., 2004b). Also, BB can enhance the emissions and long-range transport of certain non-combusted organic compounds (Medeiros et al., 2006). Sugar alcohols have been linked to airborne detritus from mature leaves and would be more prevalent during leaf senescence (Graham et al., 2003; Medeiros et al., 2006). Therefore, elevated levels of arabitol and mannitol can be expected in aerosols heavily impacted by BB during winter, supported by correlations with levoglucosan ($r = 0.39$, $p = 0.06$ for arabitol; $r = 0.40$, $p = 0.06$ for mannitol). These results suggest that BB has a greater effect on arabitol and mannitol than on glycerol, indicating their primary sources in the region may differ.

3.3.3 Biogenic SOA tracers

The total levels of biogenic SOA tracers were in the range of 1.80–34.7 ng m^{-3}, with higher concentrations in the second episode (averaging 15.8 ng m^{-3}) as shown in Fig. 4. Isoprene-derived SOA tracers accounted for a larger portion of the total biogenic SOA than combined contributions from monoterpenes and sesquiterpenes (Fig. S10). The average ratios of isoprene to monoterpene oxidation products for three episodes were 1.16 ± 0.53, 1.44 ± 0.71, and 2.16 ± 0.94, respectively. These values were lower than those reported in mountain aerosols from Central East China (about 4.9–6.7) (Fu et al., 2010), where large isoprene fluxes and high levels of atmospheric radicals like OH exist.

Isoprene, primarily emitted by terrestrial vegetation, is the predominant biogenic source of hydrocarbons in the atmosphere, though monoterpene emissions are universal among plants (Sharkey et al., 2008). Due to its reactive double bonds, isoprene can be easily oxidized by radicals (e.g., OH) contributing to tropospheric O_3 and SOA formation (Chameides et al., 1988; Claeys et al., 2004; Lin et al., 2013a). In this study, six isoprene-SOA tracers were identified: three C5-alkene triols, two 2-methyltetrols, and 2-methylglyceric acid (Table 1 and Figs. S11-S12). All tracers showed generally higher levels during the second episode, with average concentrations of 8.58 ± 2.52 ng m^{-3} for total isoprene-SOA, 2.20 ± 0.56 ng m^{-3} for C5-alkene

triols, 3.81 ± 1.20 ng m^{-3} for 2-methyltetrols (2-MTs), and 2.56 ± 0.96 ng m^{-3} for 2-methylglyceric acid (2-MGA). Analyzing the temporal variations in meteorological factors and biogenic SOA concentrations reveals that peak levels typically occurred under relatively high temperatures and low RH, in agreement with findings from central China (Li et al., 2013). The similar variation patterns among isoprene SOA tracers suggest they may originate from common sources and undergo similar formation pathways, as evidenced by significant correlations between C5-alkene triols and 2-MTs/2-MGA (r = 0.89–0.90, $p < 0.01$). Among these, 2-methyltetrols were the dominant isoprene products (0.20–8.71 ng m^{-3}), in line with previous studies (Kang et al., 2018a; Li et al., 2018). Both 2-methyltetrols and C5-alkene triols result from isoprene photooxidation under low-NO_x (NO_x = NO+NO_2) conditions (Surratt et al., 2006, 2010), while 2-MGA is formed under high-NO_x conditions (Lin et al., 2013b; Surratt et al., 2006). The concentration ratios of C5-alkene triols to 2-methyltetrols remained relatively stable, except during the most polluted episode (Fig. S13), suggesting differing reaction processes during heavy haze compared to moderate and light haze episodes. This discrepancy may arise from the chemical structure of the two species: C5-alkene triols, with their reactive double bonds, are more susceptible to oxidation. Consequently, the decreasing ratios of C5-alkene triols to 2-methyltetrols probably reflect the photochemical aging of organic aerosols over time.

Oxidation products of monoterpene include 3-hydroxyglutaricc acid (3-HGA), pinonic acid, and pinic acid. Total monoterpene-derived SOA concentrations were in the range of 1.17–13.5 ng m^{-3}, with higher levels in the second episode, likely resulting from enhanced photooxidation due to increased temperature and declined RH. An obvious correlation was found between 3-HGA and pinonic acid (r = 0.79, $p < 0.01$), implying similar sources and formation pathways. Pinic acid is a minor component of monoterpene-derived SOA (0.04–1.81 ng m^{-3}), with concentrations lower than those of 3-HGA (0.42–6.60 ng m^{-3}) and pinonic acid (0.05–6.91 ng m^{-3}). Additionally, pinic acid correlated with lignin and resin acids, such as vanillic acid and 4-HBA (r = 0.69–0.76, $p < 0.01$), suggesting BB significantly enhances its secondary formation. This is because BB serves as both an important source of air pollutants and a contributor to oxidant production (Chang et al., 2024), which increase oxidation capacity and promote

photochemistry and SOA formation. However, pinic acid did not exhibit the highest concentration during heavy haze episode, despite the significant contribution from BB. This may be due to pinic acid undergoing further reactions at high RH, forming highly oxidized polar compounds through water addition and the opening of the dimethylcyclobutane ring (Claeys et al., 2007).

β-Caryophylinic acid is a product of the ozonolysis or photooxidation of β-caryophyllene (Jaoui et al., 2007), a major species of sesquiterpenes emitted by plants (Duhl et al., 2008). Overall, β-caryophylinic acid showed a slightly higher average concentration of 0.29 ng m^{-3} during the lowest-$PM_{2.5}$ event (< 100 μg m^{-3}).

3.3.4 Aromatic acids

Three aromatic acids, including phthalic acid, isophthalic acid, and benzoic acid, were determined in these aerosols. Total aromatic acid concentrations were higher during high-$PM_{2.5}$ episodes (> 100 μg m^{-3}), ranging from 8.3 to 45.1 ng m^{-3}. Phthalic acid (Ph) and isophthalic acid (iPh) were the predominant aromatic acids, with concentrations of 1.45–13.0 ng m^{-3} and 0.98–21.2 ng m^{-3}, respectively. Secondary photochemical reactions of polycyclic aromatic hydrocarbons (PAHs), such as naphthalene, are likely primary sources of Ph, which is recognized as a naphthalene-derived SOA tracer (Fine et al., 2004; Ren et al., 2020). Vehicle exhaust is a significant source of naphthalene in urban areas, suggesting that transportation emissions contributed to Ph levels at this site. By comparison, benzoic acid was a minor component in aromatic acids (0.47–11.4 ng m^{-3}). It can be directly emitted from vehicle exhaust or formed through the photochemical reactions of aromatic hydrocarbons such as toluene (Ho et al., 2015; Li et al., 2022; Rogge et al., 1993; Suh et al., 2003). The relationships among Ph, iPh, and benzoic acid ($r = 0.64–0.79$, $p < 0.01$) suggest they share common sources, such as fossil fuels.

3.3.5 Hydroxy-/polyacids

Polyacids are reported to be secondary photooxidation products of atmospheric organic precursors (Fu et al., 2008; Kawamura and Sakaguchi, 1999). In this study, three hydroxy-/polyacids were measured, including glyceric acid, malic acid, and tartaric acid. Malic acid

(0.77–6.60 ng m^{-3}) was the major compound among the hydroxy carboxylic acids, followed by glyceric acid (0.22–6.56 ng m^{-3}), while tartaric acid presented in smaller amounts. This finding is consistent with earlier reports from the polluted East Asia/Pacific region (Simoneit et al., 2004a). A significant correlation was observed between glyceric and tartaric acid ($r = 0.81$, $p < 0.01$), suggesting similar sources and/or formation pathways. Moreover, glyceric and tartaric acid were significantly correlated with isoprene ($r = 0.71–0.93$, $p < 0.01$) and monoterpene SOA tracers (e.g., 2-methyltetrols, C5-alkene triols, pinic, and pinonic acids) ($r = 0.65–0.77$, $p < 0.01$). Malic acid showed a positive correlation with glucose ($r = 0.65$, $p < 0.01$). These significant relationships indicate that hydroxy-acids may be secondary oxidation products of biogenic VOCs and sugars (Simoneit et al., 2004a). Furthermore, glyceric acid exhibited clear correlations with aromatic acids such as iPh and benzoic acids ($r = 0.63–0.71$, $p < 0.01$), implying they may undergo similar atmospheric processing pathways. Glyceric and tartaric acids were also significantly correlated with 4-HBA and vanillic acid ($r = 0.58–0.81$, $p < 0.01$), indicating that BB contributes to their secondary production.

3.4 Contributions of primary and secondary sources to OC

To evaluate the contributions of primary sources (e.g., BB, fungal spores, and plant debris) and secondary sources (e.g., oxidation reactions of PAHs and biogenic VOCs like isoprene, monoterpene, and sesquiterpene) to OC in $PM_{2.5}$, tracer-based methods were utilized. Detailed calculations and relevant conversion factors are available in our previous studies and other literature (Bauer et al., 2008a; Gelencsér et al., 2007; Holden et al., 2011; Kang et al., 2018a; Kleindienst et al., 2007, 2012; Puxbaum and Tenze-Kunit, 2003). The results are presented in Figs. 5-6 and Table 2.

Compared to other primary and secondary sources, BB made a predominant contribution to aerosol OC throughout the sampling period, both in terms of concentration (0.72–8.86 μg m^{-3}) and proportion (8.29–26.5%). The most significant impact of BB occurred during heavy haze episode, with a mean concentration of 5.79 ± 1.50 μg m^{-3} and a contribution of 16.3% ± 3.4%. This could be linked to heightened domestic wood/crop combustion for heating and cooking, as well as open BB in nearby areas, driven by lower temperatures and higher RH during this episode (Figs. S1-S2). BB-chlorine emissions can elevate O_3 and OH radical levels,

499 significantly influencing oxidation processes (Chang et al., 2024). Besides, soluble organic
500 gases from BB can dissolve in aerosol/cloud liquid water, reacting with aqueous phase oxidants
501 to form SOA, particularly as RH increases (Zhang et al., 2024). All these findings suggest BB's
502 critical role in atmospheric chemistry and aerosol formation. Considering the potential
503 atmospheric degradation of levoglucosan, BB's contribution might be somewhat
504 underestimated, indicating that its actual fraction is likely larger. A higher BB contribution to
505 organic aerosols during colder period, characterized by elevated $PM_{2.5}$ concentrations, was also
506 recently reported in northern India (Bhattu et al., 2024). The concentration of fungal-spore-
507 derived OC was generally higher (0.44 ± 0.14 μg m^{-3}) during the highest-$PM_{2.5}$ episode,
508 coinciding with significant BB during that time (Fig. S14). This finding aligns with earlier
509 research that reported elevated fungal spore tracers on BB-affected days (Yang et al., 2012),
510 indicating that BB may enhance emissions from other sources, such as fungal spores,
511 exacerbating air pollution. However, the percentage of fungal-spore-derived OC declined with
512 increasing $PM_{2.5}$ levels, with higher fractions noted during light haze episode ($2.38\% \pm 2.26\%$),
513 when BB's contribution to OC remained substantial ($15.9\% \pm 7.01\%$). By comparison, OC from
514 plant debris was higher in the second episode (0.45 ± 0.21 μg m^{-3}, $1.99\% \pm 1.02\%$), likely due
515 to increased resuspension of surface soils and road dust resulting from elevated wind speeds
516 and temperatures (Simoneit et al., 2004b). Overall, the total abundance of primary OC derived
517 from BB, fungal spores and plant debris ranged from 1.23 to 9.65 μg m^{-3}, comprising 11.3–
518 31.3% of OC, with higher concentrations in the most polluted episode (average: 6.52 ± 1.62 μg
519 m^{-3}). Even though total primary OC concentrations were lower during light haze episodes
520 ($PM_{2.5} < 100$ μg m^{-3}), the contribution of primary OC to aerosol OC was comparable to, and
521 even exceeded ($19.9\% \pm 8.31\%$), the contributions observed in heavy and moderate episodes.

522 Secondary sources, such as isoprene, monoterpene, sesquiterpene, and naphthalene, contributed
523 only 0.38–3.56% of OC in $PM_{2.5}$, likely due to reduced photolysis during winter when sunlight
524 is less intense. Overall, SOC showed higher levels (0.36 ± 0.07 μg m^{-3}) and contributions (1.53%
525 ± 0.37%) during episodes characterized by higher temperatures and lower RH, as such weather
526 conditions enhance photochemical reactions and SOC production. Notably, naphthalene-
527 derived SOC was the primary secondary source of OC, both in concentration (0.04–0.34 μg m^{-}

528 ^{3}) and in proportion (0.27–2.46%), followed by biogenic isoprene-derived SOC (0.003–0.09 μg
529 m^{-3}, 0.01–0.60%) (Table 2). This indicates that anthropogenic VOCs predominantly contribute
530 to SOC in urban aerosols. Moreover, the total concentrations and fractional contributions of
531 biogenic SOCs (0.01–0.16 μg m^{-3}, 0.05–1.10%) were lower than those from anthropogenic
532 sources, probably due to significantly reduced biogenic VOC emissions and increased fossil
533 fuel combustion during cold winter months. The abundance and percentage of total primary and
534 secondary OC were in the range of 1.54–9.98 μg m^{-3} and 11.9–32.2%, respectively, based on
535 the tracers identified in this study. These values are comparable to those reported for winter
536 aerosol in Beijing (6.18–38.3%) (Li et al., 2018).

537 **4. Conclusions**

538 Molecular distributions and high temporal variations of primary and secondary components in
539 $PM_{2.5}$ during winter hazy episodes in urban Nanjing were comprehensively characterized
540 through intensive sampling. Our results revealed that OM dominated the total $PM_{2.5}$, followed
541 by NO_3^-. ^{14}C analysis showed that while fossil fuel sources primarily contributed to WSOC,
542 non-fossil sources, notably BB, became more significant as $PM_{2.5}$ pollution intensified. BB
543 made a dominant contribution to OC, particularly during severe haze events, likely due to
544 increased oxidants and aqueous SOA formation from BB-derived gases, with this effect
545 becoming more significant under polluted conditions with high RH and low temperatures. Other
546 non-fossil sources like fungal spore emissions were also elevated by BB, whereas plant debris
547 contributions were higher on lighter hazy days with higher wind speeds and temperatures.
548 Overall, these findings highlight the significant role of BB in winter haze over Nanjing and
549 underscore the need for further research into the molecular-level identification of gaseous
550 species from BB emissions and their role in secondary aerosol formation. Additionally,
551 although meteorological parameters have an important influence on the development of heavy
552 haze, accurately quantifying their contribution remains a challenge for future research.
553
554 **Data availability**. The dataset for this paper is available upon request from the corresponding
555 author (zhangyanlin@nuist.edu.cn).

Supplement. Information on other $PM_{2.5}$ components, including chloride, monocarboxylic acids, dicarboxylic acids, methylglyoxal, and methanesulfonic acid (MSA), is provided here, with their concentrations presented in Table S1. HYSPLIT backward trajectories initiated over Nanjing (Fig. S1). Time series of meteorological parameters (Fig. S2). Relationship between EC and OC in $PM_{2.5}$ (Fig. S3). Temporal variations of fossil and non-fossil contribution to WSOC (Fig. S4). Temporal variations of biomass burning tracers (Fig. S5). Average concentrations of anhydrosugars and lignin and resin products for three episodes (Fig. S6). Temporal variations of ratios of L/M, L/OC, and L/EC, and the average ratios during three episodes (Fig. S7). Comparison of L/M and M/G ratios between literature values and aerosols from this study (Fig. S8). Temporal variations of sugars and sugar alcohols (Fig. S9). Average and temporal concentrations of biogenic SOA tracers during three episodes (Figs. S10-S12). Temporal variations in the concentration ratios of isoprene oxidation products (Fig. S13). Temporal variations in the biogenic SOC derived from isoprene, monoterpene, and sesquiterpene (Fig. S14). Temporal variations in biomass burning-derived OC, fungal spores-derived OC, and plant debris-derived OC (Fig. S15).

Author contributions. YLZ designed the research. MYB collected aerosol samples. MYB and WHS performed the laboratory analyses. The paper was written by MJK with editing from all co-authors.

Competing interests. The authors declare that they have no conflict of interest.

Acknowledgments

This work was supported by the National Natural Science Foundation of China (No. 42192512, 42273087, and 42307142).

References

Alexeeff, S. E., Deosaransingh, K., Van Den Eeden, S., Schwartz, J., Liao, N. S., and Sidney, S.: Association of Long-term Exposure to Particulate Air Pollution With Cardiovascular Events in California, JAMA Network Open, 6, e230561, https://doi.org/10.1001/jamanetworkopen.2023.0561, 2023.

Andreae, M. O. and Merlet, P.: Emission of trace gases and aerosols from biomass burning, Global Biogeochemical Cycles, 15, 955–966, https://doi.org/10.1029/2000GB001382, 2001.

Anon: Biomass burning — a review of organic tracers for smoke from incomplete combustion, Applied Geochemistry, 17, 129–162, https://doi.org/10.1016/S0883-2927(01)00061-0, 2002.

Bao, M., Zhang, Y.-L., Cao, F., Lin, Y.-C., Hong, Y., Fan, M., Zhang, Y., Yang, X., and Xie, F.: Light absorption and source apportionment of water soluble humic-like substances (HULIS) in PM2.5 at Nanjing, China, Environmental Research, 206, 112554, https://doi.org/10.1016/j.envres.2021.112554, 2022.

Bao, M., Zhang, Y.-L., Cao, F., Hong, Y., Lin, Y.-C., Yu, M., Jiang, H., Cheng, Z., Xu, R., and Yang, X.: Impact of fossil and non-fossil fuel sources on the molecular compositions of water-soluble humic-like substances in $PM_{2.5}$ at a suburban site of Yangtze River Delta, China, Atmospheric Chemistry and Physics, 23, 8305–8324, https://doi.org/10.5194/acp-23-8305-2023, 2023.

Bauer, H., Claeys, M., Vermeylen, R., Schueller, E., Weinke, G., Berger, A., and Puxbaum, H.: Arabitol and mannitol as tracers for the quantification of airborne fungal spores, Atmospheric Environment, 42, 588–593, https://doi.org/10.1016/j.atmosenv.2007.10.013, 2008a.

Bauer, H., Schueller, E., Weinke, G., Berger, A., Hitzenberger, R., Marr, I. L., and Puxbaum, H.: Significant contributions of fungal spores to the organic carbon and to the aerosol mass balance of the urban atmospheric aerosol, Atmospheric Environment, 42, 5542–5549, https://doi.org/10.1016/j.atmosenv.2008.03.019, 2008b.

Bhattu, D., Tripathi, S. N., Bhowmik, H. S., Moschos, V., Lee, C. P., Rauber, M., Salazar, G., Abbaszade, G., Cui, T., Slowik, J. G., Vats, P., Mishra, S., Lalchandani, V., Satish, R., Rai, P., Casotto, R., Tobler, A., Kumar, V., Hao, Y., Qi, L., Khare, P., Manousakas, M. I., Wang, Q., Han, Y., Tian, J., Darfeuil, S., Minguillon, M. C., Hueglin, C., Conil, S., Rastogi, N., Srivastava, A. K., Ganguly, D., Bjelic, S., Canonaco, F., Schnelle-Kreis, J., Dominutti, P. A., Jaffrezo, J.-L., Szidat, S., Chen, Y., Cao, J., Baltensperger, U., Uzu, G., Daellenbach, K. R., El Haddad, I., and Prévôt, A. S. H.: Local incomplete combustion emissions define the PM2.5 oxidative potential in Northern India, Nat Commun, 15, 3517, https://doi.org/10.1038/s41467-024-47785-5, 2024.

Boreddy, S. K. R., Haque, M. M., and Kawamura, K.: Long-term (2001–2012) trends of carbonaceous aerosols from a remote island in the western North Pacific: an outflow region of Asian pollutants, Atmospheric Chemistry and Physics, 18, 1291–1306, https://doi.org/10.5194/acp-18-1291-2018, 2018.

Chameides, W. L., Lindsay, R. W., Richardson, J., and Kiang, C. S.: The Role of Biogenic Hydrocarbons in Urban Photochemical Smog: Atlanta as a Case Study, Science, 241, 1473–1475, https://doi.org/10.1126/science.3420404, 1988.

Chang, D., Li, Q., Wang, Z., Dai, J., Fu, X., Guo, J., Zhu, L., Pu, D., Cuevas, C. A., Fernandez, R. P., Wang, W., Ge, M., Fung, J. C. H., Lau, A. K. H., Granier, C., Brasseur, G., Pozzer, A., Saiz-Lopez, A., Song, Y., and Wang, T.: Significant chlorine emissions from biomass burning affect the long-term atmospheric chemistry in Asia, National Science Review, nwae285, https://doi.org/10.1093/nsr/nwae285, 2024.

631 Chang, X., Wang, S., Zhao, B., Xing, J., Liu, X., Wei, L., Song, Y., Wu, W., Cai, S., Zheng, H.,
632 Ding, D., and Zheng, M.: Contributions of inter-city and regional transport to PM2.5
633 concentrations in the Beijing-Tianjin-Hebei region and its implications on regional joint
634 air pollution control, Science of The Total Environment, 660, 1191–1200,
635 https://doi.org/10.1016/j.scitotenv.2018.12.474, 2019.
636 Chen, D., Liu, X., Lang, J., Zhou, Y., Wei, L., Wang, X., and Guo, X.: Estimating the
637 contribution of regional transport to PM2.5 air pollution in a rural area on the North China
638 Plain, Science of The Total Environment, 583, 280–291,
639 https://doi.org/10.1016/j.scitotenv.2017.01.066, 2017a.
640 Chen, J., Li, C., Ristovski, Z., Milic, A., Gu, Y., Islam, M. S., Wang, S., Hao, J., Zhang, H., He,
641 C., Guo, H., Fu, H., Miljevic, B., Morawska, L., Thai, P., Lam, Y. F., Pereira, G., Ding, A.,
642 Huang, X., and Dumka, U. C.: A review of biomass burning: Emissions and impacts on air
643 quality, health and climate in China, Science of The Total Environment, 579, 1000–1034,
644 https://doi.org/10.1016/j.scitotenv.2016.11.025, 2017b.
645 Chen, R., Jiang, Y., Hu, J., Chen, H., Li, H., Meng, X., Ji, J. S., Gao, Y., Wang, W., Liu, C.,
646 Fang, W., Yan, H., Chen, J., Wang, W., Xiang, D., Su, X., Yu, B., Wang, Y., Xu, Y., Wang,
647 L., Li, C., Chen, Y., Bell, M. L., Cohen, A. J., Ge, J., Huo, Y., and Kan, H.: Hourly Air
648 Pollutants and Acute Coronary Syndrome Onset in 1.29 Million Patients, Circulation, 145,
649 1749–1760, https://doi.org/10.1161/CIRCULATIONAHA.121.057179, 2022.
650 Cheng, Y., Engling, G., He, K.-B., Duan, F.-K., Ma, Y.-L., Du, Z.-Y., Liu, J.-M., Zheng, M., and
651 Weber, R. J.: Biomass burning contribution to Beijing aerosol, Atmospheric Chemistry and
652 Physics, 13, 7765–7781, https://doi.org/10.5194/acp-13-7765-2013, 2013.
653 Cheng, Y., Zheng, G., Wei, C., Mu, Q., Zheng, B., Wang, Z., Gao, M., Zhang, Q., He, K.,
654 Carmichael, G., Pöschl, U., and Su, H.: Reactive nitrogen chemistry in aerosol water as a
655 source of sulfate during haze events in China, Science Advances, 2, e1601530,
656 https://doi.org/10.1126/sciadv.1601530, 2016.
657 Claeys, M., Graham, B., Vas, G., Wang, W., Vermeylen, R., Pashynska, V., Cafmeyer, J., Guyon,
658 P., Andreae, M. O., Artaxo, P., and Maenhaut, W.: Formation of Secondary Organic
659 Aerosols Through Photooxidation of Isoprene, Science, 303, 1173–1176,
660 https://doi.org/10.1126/science.1092805, 2004.
661 Claeys, M., Szmigielski, R., Kourtchev, I., Van der Veken, P., Vermeylen, R., Maenhaut, W.,
662 Jaoui, M., Kleindienst, T. E., Lewandowski, M., Offenberg, J. H., and Edney, E. O.:
663 Hydroxydicarboxylic Acids: Markers for Secondary Organic Aerosol from the
664 Photooxidation of α-Pinene, Environ. Sci. Technol., 41, 1628–1634,
665 https://doi.org/10.1021/es0620181, 2007.
666 Ding, X., Zhang, Y.-Q., He, Q.-F., Yu, Q.-Q., Wang, J.-Q., Shen, R.-Q., Song, W., Wang, Y.-S.,
667 and Wang, X.-M.: Significant Increase of Aromatics-Derived Secondary Organic Aerosol
668 during Fall to Winter in China, Environ. Sci. Technol., 51, 7432–7441,
669 https://doi.org/10.1021/acs.est.6b06408, 2017.
670 Duhl, T. R., Helmig, D., and Guenther, A.: Sesquiterpene emissions from vegetation: a review,
671 Biogeosciences, 5, 761–777, https://doi.org/10.5194/bg-5-761-2008, 2008.
672 Elias, V. O., Simoneit, B. R. T., Cordeiro, R. C., and Turcq, B.: Evaluating levoglucosan as an
673 indicator of biomass burning in Carajás, amazônia: a comparison to the charcoal record2,

Geochimica et Cosmochimica Acta, 65, 267–272, https://doi.org/10.1016/S0016-7037(00)00522-6, 2001.

Fan, M.-Y., Zhang, Y.-L., Lin, Y.-C., Cao, F., Zhao, Z.-Y., Sun, Y., Qiu, Y., Fu, P., and Wang, Y.: Changes of Emission Sources to Nitrate Aerosols in Beijing After the Clean Air Actions: Evidence From Dual Isotope Compositions, Journal of Geophysical Research: Atmospheres, 125, e2019JD031998, https://doi.org/10.1029/2019JD031998, 2020.

Fan, M.-Y., Zhang, W., Zhang, Y.-L., Li, J., Fang, H., Cao, F., Yan, M., Hong, Y., Guo, H., and Michalski, G.: Formation Mechanisms and Source Apportionments of Nitrate Aerosols in a Megacity of Eastern China Based On Multiple Isotope Observations, Journal of Geophysical Research: Atmospheres, 128, e2022JD038129, https://doi.org/10.1029/2022JD038129, 2023.

Fine, P. M., Chakrabarti, B., Krudysz, M., Schauer, J. J., and Sioutas, C.: Diurnal Variations of Individual Organic Compound Constituents of Ultrafine and Accumulation Mode Particulate Matter in the Los Angeles Basin, Environ. Sci. Technol., 38, 1296–1304, https://doi.org/10.1021/es0348389, 2004.

Fu, P., Kawamura, K., Okuzawa, K., Aggarwal, S. G., Wang, G., Kanaya, Y., and Wang, Z.: Organic molecular compositions and temporal variations of summertime mountain aerosols over Mt. Tai, North China Plain, Journal of Geophysical Research: Atmospheres, 113, https://doi.org/10.1029/2008JD009900, 2008.

Fu, P., Kawamura, K., Kanaya, Y., and Wang, Z.: Contributions of biogenic volatile organic compounds to the formation of secondary organic aerosols over Mt. Tai, Central East China, Atmospheric Environment, 44, 4817–4826, https://doi.org/10.1016/j.atmosenv.2010.08.040, 2010.

Fu, P., Kawamura, K., Kobayashi, M., and Simoneit, B. R. T.: Seasonal variations of sugars in atmospheric particulate matter from Gosan, Jeju Island: Significant contributions of airborne pollen and Asian dust in spring, Atmospheric Environment, 55, 234–239, https://doi.org/10.1016/j.atmosenv.2012.02.061, 2012.

Fu, P., Kawamura, K., Chen, J., and Miyazaki, Y.: Secondary production of organic aerosols from biogenic VOCs over Mt. Fuji, Japan, Environmental science & technology, 48, 8491–8497, 2014.

Fu, P., Zhuang, G., Sun, Y., Wang, Q., Chen, J., Ren, L., Yang, F., Wang, Z., Pan, X., Li, X., and Kawamura, K.: Molecular markers of biomass burning, fungal spores and biogenic SOA in the Taklimakan desert aerosols, Atmospheric Environment, 130, 64–73, https://doi.org/10.1016/j.atmosenv.2015.10.087, 2016.

Gelencsér, A., May, B., Simpson, D., Sánchez-Ochoa, A., Kasper-Giebl, A., Puxbaum, H., Caseiro, A., Pio, C., and Legrand, M.: Source apportionment of PM2.5 organic aerosol over Europe: Primary/secondary, natural/anthropogenic, and fossil/biogenic origin, Journal of Geophysical Research: Atmospheres, 112, https://doi.org/10.1029/2006JD008094, 2007.

Gilardoni, S., Massoli, P., Paglione, M., Giulianelli, L., Carbone, C., Rinaldi, M., Decesari, S., Sandrini, S., Costabile, F., Gobbi, G. P., Pietrogrande, M. C., Visentin, M., Scotto, F., Fuzzi, S., and Facchini, M. C.: Direct observation of aqueous secondary organic aerosol from biomass-burning emissions, Proceedings of the National Academy of Sciences, 113, 10013–10018, https://doi.org/10.1073/pnas.1602212113, 2016.

718 Graham, B., Guyon, P., Taylor, P. E., Artaxo, P., Maenhaut, W., Glovsky, M. M., Flagan, R. C.,
719 and Andreae, M. O.: Organic compounds present in the natural Amazonian aerosol:
720 Characterization by gas chromatography–mass spectrometry, Journal of Geophysical
721 Research: Atmospheres, 108, https://doi.org/10.1029/2003JD003990, 2003.
722 Griffin, R. J., Cocker III, D. R., Seinfeld, J. H., and Dabdub, D.: Estimate of global atmospheric
723 organic aerosol from oxidation of biogenic hydrocarbons, Geophysical Research Letters,
724 26, 2721–2724, https://doi.org/10.1029/1999GL900476, 1999.
725 Guenther, A., Karl, T., Harley, P., Wiedinmyer, C., Palmer, P. I., and Geron, C.: Estimates of
726 global terrestrial isoprene emissions using MEGAN (Model of Emissions of Gases and
727 Aerosols from Nature), Atmospheric Chemistry and Physics, 6, 3181–3210,
728 https://doi.org/10.5194/acp-6-3181-2006, 2006.
729 Hallquist, M., Wenger, J. C., Baltensperger, U., Rudich, Y., Simpson, D., Claeys, M., Dommen,
730 J., Donahue, N. M., George, C., Goldstein, A. H., Hamilton, J. F., Herrmann, H., Hoffmann,
731 T., Iinuma, Y., Jang, M., Jenkin, M. E., Jimenez, J. L., Kiendler-Scharr, A., Maenhaut, W.,
732 McFiggans, G., Mentel, T. F., Monod, A., Prévôt, A. S. H., Seinfeld, J. H., Surratt, J. D.,
733 Szmigielski, R., and Wildt, J.: The formation, properties and impact of secondary organic
734 aerosol: current and emerging issues, Atmospheric Chemistry and Physics, 9, 5155–5236,
735 https://doi.org/10.5194/acp-9-5155-2009, 2009.
736 Ho, K. F., Huang, R.-J., Kawamura, K., Tachibana, E., Lee, S. C., Ho, S. S. H., Zhu, T., and
737 Tian, L.: Dicarboxylic acids, ketocarboxylic acids, α-dicarbonyls, fatty acids and benzoic
738 acid in $PM_{2.5}$ aerosol collected during CAREBeijing-2007: an effect of traffic restriction
739 on air quality, Atmospheric Chemistry and Physics, 15, 3111–3123,
740 https://doi.org/10.5194/acp-15-3111-2015, 2015.
741 Holden, A. S., Sullivan, A. P., Munchak, L. A., Kreidenweis, S. M., Schichtel, B. A., Malm, W.
742 C., and Collett, J. L.: Determining contributions of biomass burning and other sources to
743 fine particle contemporary carbon in the western United States, Atmospheric Environment,
744 45, 1986–1993, https://doi.org/10.1016/j.atmosenv.2011.01.021, 2011.
745 Huang, R.-J., Zhang, Y., Bozzetti, C., Ho, K.-F., Cao, J.-J., Han, Y., Daellenbach, K. R., Slowik,
746 J. G., Platt, S. M., Canonaco, F., Zotter, P., Wolf, R., Pieber, S. M., Bruns, E. A., Crippa,
747 M., Ciarelli, G., Piazzalunga, A., Schwikowski, M., Abbaszade, G., Schnelle-Kreis, J.,
748 Zimmermann, R., An, Z., Szidat, S., Baltensperger, U., Haddad, I. E., and Prévôt, A. S. H.:
749 High secondary aerosol contribution to particulate pollution during haze events in China,
750 Nature, 514, 218–222, https://doi.org/10.1038/nature13774, 2014.
751 Huang, X., Ding, A., Wang, Z., Ding, K., Gao, J., Chai, F., and Fu, C.: Amplified transboundary
752 transport of haze by aerosol–boundary layer interaction in China, Nat. Geosci., 13, 428–
753 434, https://doi.org/10.1038/s41561-020-0583-4, 2020a.
754 Huang, X., Ding, A., Gao, J., Zheng, B., Zhou, D., Qi, X., Tang, R., Wang, J., Ren, C., Nie, W.,
755 Chi, X., Xu, Z., Chen, L., Li, Y., Che, F., Pang, N., Wang, H., Tong, D., Qin, W., Cheng,
756 W., Liu, W., Fu, Q., Liu, B., Chai, F., Davis, S. J., Zhang, Q., and He, K.: Enhanced
757 secondary pollution offset reduction of primary emissions during COVID-19 lockdown in
758 China, National Science Review, https://doi.org/10.1093/nsr/nwaa137, 2020b.
759 Jaoui, M., Lewandowski, M., Kleindienst, T. E., Offenberg, J. H., and Edney, E. O.: β-
760 caryophyllinic acid: An atmospheric tracer for β-caryophyllene secondary organic aerosol,
761 Geophysical Research Letters, 34, https://doi.org/10.1029/2006GL028827, 2007.

762 Ji, D., Gao, W., Maenhaut, W., He, J., Wang, Z., Li, J., Du, W., Wang, L., Sun, Y., Xin, J., Hu,
763 B., and Wang, Y.: Impact of air pollution control measures and regional transport on
764 carbonaceous aerosols in fine particulate matter in urban Beijing, China: insights gained
765 from long-term measurement, Atmospheric Chemistry and Physics, 19, 8569–8590,
766 https://doi.org/10.5194/acp-19-8569-2019, 2019.
767 Jia, Y. and Fraser, M.: Characterization of Saccharides in Size-fractionated Ambient Particulate
768 Matter and Aerosol Sources: The Contribution of Primary Biological Aerosol Particles
769 (PBAPs) and Soil to Ambient Particulate Matter, Environ. Sci. Technol., 45, 930–936,
770 https://doi.org/10.1021/es103104e, 2011.
771 Jimenez, J. L., Canagaratna, M. R., Donahue, N. M., Prevot, A. S. H., Zhang, Q., Kroll, J. H.,
772 DeCarlo, P. F., Allan, J. D., Coe, H., Ng, N. L., Aiken, A. C., Docherty, K. S., Ulbrich, I.
773 M., Grieshop, A. P., Robinson, A. L., Duplissy, J., Smith, J. D., Wilson, K. R., Lanz, V. A.,
774 Hueglin, C., Sun, Y. L., Tian, J., Laaksonen, A., Raatikainen, T., Rautiainen, J., Vaattovaara,
775 P., Ehn, M., Kulmala, M., Tomlinson, J. M., Collins, D. R., Cubison, M. J., E., Dunlea, J.,
776 Huffman, J. A., Onasch, T. B., Alfarra, M. R., Williams, P. I., Bower, K., Kondo, Y.,
777 Schneider, J., Drewnick, F., Borrmann, S., Weimer, S., Demerjian, K., Salcedo, D., Cottrell,
778 L., Griffin, R., Takami, A., Miyoshi, T., Hatakeyama, S., Shimono, A., Sun, J. Y., Zhang,
779 Y. M., Dzepina, K., Kimmel, J. R., Sueper, D., Jayne, J. T., Herndon, S. C., Trimborn, A.
780 M., Williams, L. R., Wood, E. C., Middlebrook, A. M., Kolb, C. E., Baltensperger, U., and
781 Worsnop, D. R.: Evolution of Organic Aerosols in the Atmosphere, Science, 326, 1525–
782 1529, https://doi.org/10.1126/science.1180353, 2009.
783 Kanakidou, M., Seinfeld, J. H., Pandis, S. N., Barnes, I., Dentener, F. J., Facchini, M. C.,
784 Dingenen, R. V., Ervens, B., Nenes, A., Nielsen, C. J., Swietlicki, E., Putaud, J. P.,
785 Balkanski, Y., Fuzzi, S., Horth, J., Moortgat, G. K., Winterhalter, R., Myhre, C. E. L.,
786 Tsigaridis, K., Vignati, E., Stephanou, E. G., and Wilson, J.: Organic aerosol and global
787 climate modelling: a review, Atmospheric Chemistry and Physics, 5, 1053–1123,
788 https://doi.org/10.5194/acp-5-1053-2005, 2005.
789 Kang, M., Fu, P., Aggarwal, S. G., Kumar, S., Zhao, Y., Sun, Y., and Wang, Z.: Size distributions
790 of n-alkanes, fatty acids and fatty alcohols in springtime aerosols from New Delhi, India,
791 Environmental Pollution, 219, 957–966, https://doi.org/10.1016/j.envpol.2016.09.077,
792 2016.
793 Kang, M., Fu, P., Kawamura, K., Yang, F., Zhang, H., Zang, Z., Ren, H., Ren, L., Zhao, Y., Sun,
794 Y., and Wang, Z.: Characterization of biogenic primary and secondary organic aerosols in
795 the marine atmosphere over the East China Sea, Atmospheric Chemistry and Physics, 18,
796 13947–13967, https://doi.org/10.5194/acp-18-13947-2018, 2018a.
797 Kang, M., Ren, L., Ren, H., Zhao, Y., Kawamura, K., Zhang, H., Wei, L., Sun, Y., Wang, Z.,
798 and Fu, P.: Primary biogenic and anthropogenic sources of organic aerosols in Beijing,
799 China: Insights from saccharides and n-alkanes, Environmental Pollution, 243, 1579–1587,
800 https://doi.org/10.1016/j.envpol.2018.09.118, 2018b.
801 Kang, M., Guo, H., Wang, P., Fu, P., Ying, Q., Liu, H., Zhao, Y., and Zhang, H.: Characterization
802 and source apportionment of marine aerosols over the East China Sea, Science of The Total
803 Environment, 651, 2679–2688, https://doi.org/10.1016/j.scitotenv.2018.10.174, 2019.

Kang, M., Zhang, J., Zhang, H., and Ying, Q.: On the Relevancy of Observed Ozone Increase during COVID-19 Lockdown to Summertime Ozone and PM2.5 Control Policies in China, Environ. Sci. Technol. Lett., 8, 289–294, https://doi.org/10.1021/acs.estlett.1c00036, 2021.

Kaufman, Y. J., Tanré, D., and Boucher, O.: A satellite view of aerosols in the climate system, Nature, 419, 215–223, https://doi.org/10.1038/nature01091, 2002.

Kawamura, K. and Sakaguchi, F.: Molecular distributions of water soluble dicarboxylic acids in marine aerosols over the Pacific Ocean including tropics, Journal of Geophysical Research: Atmospheres, 104, 3501–3509, https://doi.org/10.1029/1998JD100041, 1999.

Kawana, K., Miyazaki, Y., Omori, Y., Tanimoto, H., Kagami, S., Suzuki, K., Yamashita, Y., Nishioka, J., Deng, Y., Yai, H., and Mochida, M.: Number-Size Distribution and CCN Activity of Atmospheric Aerosols in the Western North Pacific During Spring Pre-Bloom Period: Influences of Terrestrial and Marine Sources, Journal of Geophysical Research: Atmospheres, 127, e2022JD036690, https://doi.org/10.1029/2022JD036690, 2022.

Kleindienst, T. E., Jaoui, M., Lewandowski, M., Offenberg, J. H., Lewis, C. W., Bhave, P. V., and Edney, E. O.: Estimates of the contributions of biogenic and anthropogenic hydrocarbons to secondary organic aerosol at a southeastern US location, Atmospheric Environment, 41, 8288–8300, https://doi.org/10.1016/j.atmosenv.2007.06.045, 2007.

Kleindienst, T. E., Jaoui, M., Lewandowski, M., Offenberg, J. H., and Docherty, K. S.: The formation of SOA and chemical tracer compounds from the photooxidation of naphthalene and its methyl analogs in the presence and absence of nitrogen oxides, Atmospheric Chemistry and Physics, 12, 8711–8726, https://doi.org/10.5194/acp-12-8711-2012, 2012.

Le, T., Wang, Y., Liu, L., Yang, J., Yung, Y. L., Li, G., and Seinfeld, J. H.: Unexpected air pollution with marked emission reductions during the COVID-19 outbreak in China, Science, 369, 702–706, https://doi.org/10.1126/science.abb7431, 2020.

Li, B., Zhang, J., Zhao, Y., Yuan, S., Zhao, Q., Shen, G., and Wu, H.: Seasonal variation of urban carbonaceous aerosols in a typical city Nanjing in Yangtze River Delta, China, Atmospheric Environment, 106, 223–231, https://doi.org/10.1016/j.atmosenv.2015.01.064, 2015.

Li, C., Bosch, C., Kang, S., Andersson, A., Chen, P., Zhang, Q., Cong, Z., Chen, B., Qin, D., and Gustafsson, Ö.: Sources of black carbon to the Himalayan–Tibetan Plateau glaciers, Nature Communications, 7, 12574, https://doi.org/10.1038/ncomms12574, 2016a.

Li, F., Tsona, N. T., Li, J., and Du, L.: Aqueous-phase oxidation of syringic acid emitted from biomass burning: Formation of light-absorbing compounds, Science of The Total Environment, 765, 144239, https://doi.org/10.1016/j.scitotenv.2020.144239, 2021a.

Li, H., Wang, Q., Yang, M., Li, F., Wang, J., Sun, Y., Wang, C., Wu, H., and Qian, X.: Chemical characterization and source apportionment of PM2.5 aerosols in a megacity of Southeast China, Atmospheric Research, 181, 288–299, https://doi.org/10.1016/j.atmosres.2016.07.005, 2016b.

Li, J. J., Wang, G. H., Cao, J. J., Wang, X. M., and Zhang, R. J.: Observation of biogenic secondary organic aerosols in the atmosphere of a mountain site in central China: temperature and relative humidity effects, Atmospheric Chemistry and Physics, 13, 11535–11549, https://doi.org/10.5194/acp-13-11535-2013, 2013.

Li, K., Zhang, J., Bell, D. M., Wang, T., Lamkaddam, H., Cui, T., Qi, L., Surdu, M., Wang, D., Du, L., El Haddad, I., Slowik, J. G., and Prevot, A. S. H.: Uncovering the dominant

contribution of intermediate volatility compounds in secondary organic aerosol formation from biomass-burning emissions, National Science Review, 11, nwae014, https://doi.org/10.1093/nsr/nwae014, 2024.

Li, L., Ren, L., Ren, H., Yue, S., Xie, Q., Zhao, W., Kang, M., Li, J., Wang, Z., Sun, Y., and Fu, P.: Molecular Characterization and Seasonal Variation in Primary and Secondary Organic Aerosols in Beijing, China, Journal of Geophysical Research: Atmospheres, 123, 12,394-12,412, https://doi.org/10.1029/2018JD028527, 2018.

Li, X.-B., Yuan, B., Wang, S., Wang, C., Lan, J., Liu, Z., Song, Y., He, X., Huangfu, Y., Pei, C., Cheng, P., Yang, S., Qi, J., Wu, C., Huang, S., You, Y., Chang, M., Zheng, H., Yang, W., Wang, X., and Shao, M.: Variations and sources of volatile organic compounds (VOCs) in urban region: insights from measurements on a tall tower, Atmospheric Chemistry and Physics, 22, 10567–10587, https://doi.org/10.5194/acp-22-10567-2022, 2022.

Li, Y., Fu, T.-M., Yu, J. Z., Feng, X., Zhang, L., Chen, J., Boreddy, S. K. R., Kawamura, K., Fu, P., Yang, X., Zhu, L., and Zeng, Z.: Impacts of Chemical Degradation on the Global Budget of Atmospheric Levoglucosan and Its Use As a Biomass Burning Tracer, Environ. Sci. Technol., 55, 5525–5536, https://doi.org/10.1021/acs.est.0c07313, 2021b.

Li, Y. J., Huang, D. D., Cheung, H. Y., Lee, A. K. Y., and Chan, C. K.: Aqueous-phase photochemical oxidation and direct photolysis of vanillin – a model compound of methoxy phenols from biomass burning, Atmospheric Chemistry and Physics, 14, 2871–2885, https://doi.org/10.5194/acp-14-2871-2014, 2014.

Lim, C. Y., Hagan, D. H., Coggon, M. M., Koss, A. R., Sekimoto, K., de Gouw, J., Warneke, C., Cappa, C. D., and Kroll, J. H.: Secondary organic aerosol formation from the laboratory oxidation of biomass burning emissions, Atmospheric Chemistry and Physics, 19, 12797–12809, https://doi.org/10.5194/acp-19-12797-2019, 2019.

Lin, Y.-C., Zhang, Y.-L., Fan, M.-Y., and Bao, M.: Heterogeneous formation of particulate nitrate under ammonium-rich regimes during the high-$PM_{2.5}$ events in Nanjing, China, Atmospheric Chemistry and Physics, 20, 3999–4011, https://doi.org/10.5194/acp-20-3999-2020, 2020.

Lin, Y.-C., Fan, M.-Y., Hong, Y., Yu, M., Cao, F., and Zhang, Y.-L.: Important contributions of natural gas combustion to atmospheric nitrate aerosols in China: Insights from stable nitrogen isotopes, Science Bulletin, https://doi.org/10.1016/j.scib.2024.06.038, 2024.

Lin, Y.-H., Zhang, H., Pye, H. O. T., Zhang, Z., Marth, W. J., Park, S., Arashiro, M., Cui, T., Budisulistiorini, S. H., Sexton, K. G., Vizuete, W., Xie, Y., Luecken, D. J., Piletic, I. R., Edney, E. O., Bartolotti, L. J., Gold, A., and Surratt, J. D.: Epoxide as a precursor to secondary organic aerosol formation from isoprene photooxidation in the presence of nitrogen oxides, Proceedings of the National Academy of Sciences, 110, 6718–6723, https://doi.org/10.1073/pnas.1221150110, 2013a.

Lin, Y.-H., Knipping, E. M., Edgerton, E. S., Shaw, S. L., and Surratt, J. D.: Investigating the influences of SO_2 and NH_3 levels on isoprene-derived secondary organic aerosol formation using conditional sampling approaches, Atmospheric Chemistry and Physics, 13, 8457–8470, https://doi.org/10.5194/acp-13-8457-2013, 2013b.

Liu, D., Li, J., Zhang, Y., Xu, Y., Liu, X., Ding, P., Shen, C., Chen, Y., Tian, C., and Zhang, G.: The Use of Levoglucosan and Radiocarbon for Source Apportionment of PM2.5

Carbonaceous Aerosols at a Background Site in East China, Environ. Sci. Technol., 47, 10454–10461, https://doi.org/10.1021/es401250k, 2013.

Liu, J., Li, J., Zhang, Y., Liu, D., Ding, P., Shen, C., Shen, K., He, Q., Ding, X., Wang, X., Chen, D., Szidat, S., and Zhang, G.: Source Apportionment Using Radiocarbon and Organic Tracers for PM2.5 Carbonaceous Aerosols in Guangzhou, South China: Contrasting Local- and Regional-Scale Haze Events, Environ. Sci. Technol., 48, 12002–12011, https://doi.org/10.1021/es503102w, 2014.

Liu, J., Li, J., Liu, D., Ding, P., Shen, C., Mo, Y., Wang, X., Luo, C., Cheng, Z., Szidat, S., Zhang, Y., Chen, Y., and Zhang, G.: Source apportionment and dynamic changes of carbonaceous aerosols during the haze bloom-decay process in China based on radiocarbon and organic molecular tracers, Atmospheric Chemistry and Physics, 16, 2985–2996, https://doi.org/10.5194/acp-16-2985-2016, 2016.

Lu, K., Guo, S., Tan, Z., Wang, H., Shang, D., Liu, Y., Li, X., Wu, Z., Hu, M., and Zhang, Y.: Exploring atmospheric free-radical chemistry in China: the self-cleansing capacity and the formation of secondary air pollution, National Science Review, 6, 579–594, https://doi.org/10.1093/nsr/nwy073, 2019.

Medeiros, P. M., Conte, M. H., Weber, J. C., and Simoneit, B. R. T.: Sugars as source indicators of biogenic organic carbon in aerosols collected above the Howland Experimental Forest, Maine, Atmospheric Environment, 40, 1694–1705, https://doi.org/10.1016/j.atmosenv.2005.11.001, 2006.

Mochida, M., Kawamura, K., Fu, P., and Takemura, T.: Seasonal variation of levoglucosan in aerosols over the western North Pacific and its assessment as a biomass-burning tracer, Atmospheric Environment, 44, 3511–3518, https://doi.org/10.1016/j.atmosenv.2010.06.017, 2010.

Morris, C. E., Sands, D. C., Bardin, M., Jaenicke, R., Vogel, B., Leyronas, C., Ariya, P. A., and Psenner, R.: Microbiology and atmospheric processes: research challenges concerning the impact of airborne micro-organisms on the atmosphere and climate, Biogeosciences, 8, 17–25, https://doi.org/10.5194/bg-8-17-2011, 2011.

Mozaffar, A., Zhang, Y.-L., Fan, M., Cao, F., and Lin, Y.-C.: Characteristics of summertime ambient VOCs and their contributions to O3 and SOA formation in a suburban area of Nanjing, China, Atmospheric Research, 240, 104923, https://doi.org/10.1016/j.atmosres.2020.104923, 2020.

Pope, C. A., Burnett, R. T., Thurston, G. D., Thun, M. J., Calle, E. E., Krewski, D., and Godleski, J. J.: Cardiovascular Mortality and Long-Term Exposure to Particulate Air Pollution, Circulation, 109, 71–77, https://doi.org/10.1161/01.CIR.0000108927.80044.7F, 2004.

Pöschl, U., Martin, S. T., Sinha, B., Chen, Q., Gunthe, S. S., Huffman, J. A., Borrmann, S., Farmer, D. K., Garland, R. M., Helas, G., Jimenez, J. L., King, S. M., Manzi, A., Mikhailov, E., Pauliquevis, T., Petters, M. D., Prenni, A. J., Roldin, P., Rose, D., Schneider, J., Su, H., Zorn, S. R., Artaxo, P., and Andreae, M. O.: Rainforest Aerosols as Biogenic Nuclei of Clouds and Precipitation in the Amazon, Science, 329, 1513–1516, https://doi.org/10.1126/science.1191056, 2010.

Puxbaum, H. and Tenze-Kunit, M.: Size distribution and seasonal variation of atmospheric cellulose, Atmospheric Environment, 37, 3693–3699, https://doi.org/10.1016/S1352-2310(03)00451-5, 2003.

Ram, K., Sarin, M. M., and Hegde, P.: Long-term record of aerosol optical properties and chemical composition from a high-altitude site (Manora Peak) in Central Himalaya, Atmospheric Chemistry and Physics, 10, 11791–11803, https://doi.org/10.5194/acp-10-11791-2010, 2010.

Ren, G., Yan, X., Ma, Y., Qiao, L., Chen, Z., Xin, Y., Zhou, M., Shi, Y., Zheng, K., Zhu, S., Huang, C., and Li, L.: Characteristics and source apportionment of PM2.5-bound saccharides and carboxylic acids in Central Shanghai, China, Atmospheric Research, 237, 104817, https://doi.org/10.1016/j.atmosres.2019.104817, 2020.

Rivellini, L.-H., Jorga, S., Wang, Y., Lee, A. K. Y., Murphy, J. G., Chan, A. W., and Abbatt, J. P. D.: Sources of Wintertime Atmospheric Organic Pollutants in a Large Canadian City: Insights from Particle and Gas Phase Measurements, ACS EST Air, https://doi.org/10.1021/acsestair.4c00039, 2024.

Rogge, W. F., Hildemann, L. M., Mazurek, M. A., Cass, G. R., and Simoneit, B. R. T.: Sources of fine organic aerosol. 2. Noncatalyst and catalyst-equipped automobiles and heavy-duty diesel trucks, Environ. Sci. Technol., 27, 636–651, https://doi.org/10.1021/es00041a007, 1993.

Rogge, W. F., Medeiros, P. M., and Simoneit, B. R. T.: Organic marker compounds in surface soils of crop fields from the San Joaquin Valley fugitive dust characterization study, Atmospheric Environment, 41, 8183–8204, https://doi.org/10.1016/j.atmosenv.2007.06.030, 2007.

Shah, V., Keller, C. A., Knowland, K. E., Christiansen, A., Hu, L., Wang, H., Lu, X., Alexander, B., and Jacob, D. J.: Particulate Nitrate Photolysis as a Possible Driver of Rising Tropospheric Ozone, Geophysical Research Letters, 51, e2023GL107980, https://doi.org/10.1029/2023GL107980, 2024.

Sharkey, T. D., Wiberley, A. E., and Donohue, A. R.: Isoprene Emission from Plants: Why and How, Ann Bot, 101, 5–18, https://doi.org/10.1093/aob/mcm240, 2008.

Simoneit, B. R. T.: Biomass burning — a review of organic tracers for smoke from incomplete combustion, Applied Geochemistry, 17, 129–162, https://doi.org/10.1016/S0883-2927(01)00061-0, 2002.

Simoneit, B. R. T., Kobayashi, M., Mochida, M., Kawamura, K., and Huebert, B. J.: Aerosol particles collected on aircraft flights over the northwestern Pacific region during the ACE-Asia campaign: Composition and major sources of the organic compounds, Journal of Geophysical Research: Atmospheres, 109, https://doi.org/10.1029/2004JD004565, 2004a.

Simoneit, B. R. T., Elias, V. O., Kobayashi, M., Kawamura, K., Rushdi, A. I., Medeiros, P. M., Rogge, W. F., and Didyk, B. M.: SugarsDominant Water-Soluble Organic Compounds in Soils and Characterization as Tracers in Atmospheric Particulate Matter, Environ. Sci. Technol., 38, 5939–5949, https://doi.org/10.1021/es0403099, 2004b.

Sindelarova, K., Granier, C., Bouarar, I., Guenther, A., Tilmes, S., Stavrakou, T., Müller, J.-F., Kuhn, U., Stefani, P., and Knorr, W.: Global data set of biogenic VOC emissions calculated by the MEGAN model over the last 30 years, Atmospheric Chemistry and Physics, 14, 9317–9341, https://doi.org/10.5194/acp-14-9317-2014, 2014.

Song, W., Zhang, Y.-L., Zhang, Y., Cao, F., Rauber, M., Salazar, G., Kawichai, S., Prapamontol, T., and Szidat, S.: Is biomass burning always a dominant contributor of fine aerosols in

upper northern Thailand?, Environment International, 168, 107466, https://doi.org/10.1016/j.envint.2022.107466, 2022.

Srivastava, D., Vu, T. V., Tong, S., Shi, Z., and Harrison, R. M.: Formation of secondary organic aerosols from anthropogenic precursors in laboratory studies, npj Clim Atmos Sci, 5, 1–30, https://doi.org/10.1038/s41612-022-00238-6, 2022.

Suh, I., Zhang, R., Molina, L. T., and Molina, M. J.: Oxidation Mechanism of Aromatic Peroxy and Bicyclic Radicals from OH−Toluene Reactions, J. Am. Chem. Soc., 125, 12655–12665, https://doi.org/10.1021/ja0350280, 2003.

Sullivan, A. P., Holden, A. S., Patterson, L. A., McMeeking, G. R., Kreidenweis, S. M., Malm, W. C., Hao, W. M., Wold, C. E., and Collett Jr., J. L.: A method for smoke marker measurements and its potential application for determining the contribution of biomass burning from wildfires and prescribed fires to ambient PM2.5 organic carbon, Journal of Geophysical Research: Atmospheres, 113, https://doi.org/10.1029/2008JD010216, 2008.

Sun, Y., Jiang, Q., Wang, Z., Fu, P., Li, J., Yang, T., and Yin, Y.: Investigation of the sources and evolution processes of severe haze pollution in Beijing in January 2013, Journal of Geophysical Research: Atmospheres, 119, 4380–4398, https://doi.org/10.1002/2014JD021641, 2014.

Surratt, J. D., Murphy, S. M., Kroll, J. H., Ng, N. L., Hildebrandt, L., Sorooshian, A., Szmigielski, R., Vermeylen, R., Maenhaut, W., Claeys, M., Flagan, R. C., and Seinfeld, J. H.: Chemical Composition of Secondary Organic Aerosol Formed from the Photooxidation of Isoprene, J. Phys. Chem. A, 110, 9665–9690, https://doi.org/10.1021/jp061734m, 2006.

Surratt, J. D., Chan, A. W. H., Eddingsaas, N. C., Chan, M., Loza, C. L., Kwan, A. J., Hersey, S. P., Flagan, R. C., Wennberg, P. O., and Seinfeld, J. H.: Reactive intermediates revealed in secondary organic aerosol formation from isoprene, Proceedings of the National Academy of Sciences, 107, 6640–6645, https://doi.org/10.1073/pnas.0911114107, 2010.

Turpin, B. J. and Lim, H.-J.: Species Contributions to PM2.5 Mass Concentrations: Revisiting Common Assumptions for Estimating Organic Mass, Aerosol Science and Technology, 35, 602–610, https://doi.org/10.1080/02786820119445, 2001.

Urban, R. C., Lima-Souza, M., Caetano-Silva, L., Queiroz, M. E. C., Nogueira, R. F. P., Allen, A. G., Cardoso, A. A., Held, G., and Campos, M. L. A. M.: Use of levoglucosan, potassium, and water-soluble organic carbon to characterize the origins of biomass-burning aerosols, Atmospheric Environment, 61, 562–569, https://doi.org/10.1016/j.atmosenv.2012.07.082, 2012.

Virkkula, A., Teinilä, K., Hillamo, R., Kerminen, V.-M., Saarikoski, S., Aurela, M., Viidanoja, J., Paatero, J., Koponen, I. K., and Kulmala, M.: Chemical composition of boundary layer aerosol over the Atlantic Ocean and at an Antarctic site, Atmospheric Chemistry and Physics, 6, 3407–3421, https://doi.org/10.5194/acp-6-3407-2006, 2006.

Wang, G., Kawamura, K., Lee, S., Ho, K., and Cao, J.: Molecular, Seasonal, and Spatial Distributions of Organic Aerosols from Fourteen Chinese Cities, Environ. Sci. Technol., 40, 4619–4625, https://doi.org/10.1021/es060291x, 2006.

Wang, L., Li, Q., Qiu, Q., Hou, L., Ouyang, J., Zeng, R., Huang, S., Li, J., Tang, L., and Liu, Y.: Assessing the ecological risk induced by PM2.5 pollution in a fast developing urban

agglomeration of southeastern China, Journal of Environmental Management, 324, 116284, https://doi.org/10.1016/j.jenvman.2022.116284, 2022.

Wang, P., Chen, K., Zhu, S., Wang, P., and Zhang, H.: Severe air pollution events not avoided by reduced anthropogenic activities during COVID-19 outbreak, Resources, Conservation and Recycling, 158, 104814, https://doi.org/10.1016/j.resconrec.2020.104814, 2020.

Wu, X., Cao, F., Haque, M., Fan, M.-Y., Zhang, S.-C., and Zhang, Y.-L.: Molecular composition and source apportionment of fine organic aerosols in Northeast China, Atmospheric Environment, 239, 117722, https://doi.org/10.1016/j.atmosenv.2020.117722, 2020.

Xiao, Y., Hu, M., Li, X., Zong, T., Xu, N., Hu, S., Zeng, L., Chen, S., Song, Y., Guo, S., and Wu, Z.: Aqueous secondary organic aerosol formation attributed to phenols from biomass burning, Science of The Total Environment, 847, 157582, https://doi.org/10.1016/j.scitotenv.2022.157582, 2022.

Yan, C., Tham, Y. J., Nie, W., Xia, M., Wang, H., Guo, Y., Ma, W., Zhan, J., Hua, C., Li, Y., Deng, C., Li, Y., Zheng, F., Chen, X., Li, Q., Zhang, G., Mahajan, A. S., Cuevas, C. A., Huang, D. D., Wang, Z., Sun, Y., Saiz-Lopez, A., Bianchi, F., Kerminen, V.-M., Worsnop, D. R., Donahue, N. M., Jiang, J., Liu, Y., Ding, A., and Kulmala, M.: Increasing contribution of nighttime nitrogen chemistry to wintertime haze formation in Beijing observed during COVID-19 lockdowns, Nat. Geosci., 1–7, https://doi.org/10.1038/s41561-023-01285-1, 2023.

Yang, G.-P., Zhang, S.-H., Zhang, H.-H., Yang, J., and Liu, C.-Y.: Distribution of biogenic sulfur in the Bohai Sea and northern Yellow Sea and its contribution to atmospheric sulfate aerosol in the late fall, Marine Chemistry, 169, 23–32, https://doi.org/10.1016/j.marchem.2014.12.008, 2015.

Yang, T., Li, H., Xu, W., Song, Y., Xu, L., Wang, H., Wang, F., Sun, Y., Wang, Z., and Fu, P.: Strong Impacts of Regional Atmospheric Transport on the Vertical Distribution of Aerosol Ammonium over Beijing, Environ. Sci. Technol. Lett., 11, 29–34, https://doi.org/10.1021/acs.estlett.3c00791, 2024.

Yang, Y., Chan, C., Tao, J., Lin, M., Engling, G., Zhang, Z., Zhang, T., and Su, L.: Observation of elevated fungal tracers due to biomass burning in the Sichuan Basin at Chengdu City, China, Science of The Total Environment, 431, 68–77, https://doi.org/10.1016/j.scitotenv.2012.05.033, 2012.

Yee, L. D., Kautzman, K. E., Loza, C. L., Schilling, K. A., Coggon, M. M., Chhabra, P. S., Chan, M. N., Chan, A. W. H., Hersey, S. P., Crounse, J. D., Wennberg, P. O., Flagan, R. C., and Seinfeld, J. H.: Secondary organic aerosol formation from biomass burning intermediates: phenol and methoxyphenols, Atmospheric Chemistry and Physics, 13, 8019–8043, https://doi.org/10.5194/acp-13-8019-2013, 2013.

Youn, J.-S., Wang, Z., Wonaschütz, A., Arellano, A., Betterton, E. A., and Sorooshian, A.: Evidence of aqueous secondary organic aerosol formation from biogenic emissions in the North American Sonoran Desert, Geophysical Research Letters, 40, 3468–3472, https://doi.org/10.1002/grl.50644, 2013.

Zhang, H., Li, J., Ying, Q., Yu, J. Z., Wu, D., Cheng, Y., He, K., and Jiang, J.: Source apportionment of PM2.5 nitrate and sulfate in China using a source-oriented chemical transport model, Atmospheric Environment, 62, 228–242, https://doi.org/10.1016/j.atmosenv.2012.08.014, 2012.

Zhang, H., Hu, J., Kleeman, M., and Ying, Q.: Source apportionment of sulfate and nitrate particulate matter in the Eastern United States and effectiveness of emission control programs, Science of The Total Environment, 490, 171–181, https://doi.org/10.1016/j.scitotenv.2014.04.064, 2014a.

Zhang, J., He, X., Ding, X., Yu, J. Z., and Ying, Q.: Modeling Secondary Organic Aerosol Tracers and Tracer-to-SOA Ratios for Monoterpenes and Sesquiterpenes Using a Chemical Transport Model, Environ. Sci. Technol., 56, 804–813, https://doi.org/10.1021/acs.est.1c06373, 2022.

Zhang, J., Liu, J., Ding, X., He, X., Zhang, T., Zheng, M., Choi, M., Isaacman-VanWertz, G., Yee, L., Zhang, H., Misztal, P., Goldstein, A. H., Guenther, A. B., Budisulistiorini, S. H., Surratt, J. D., Stone, E. A., Shrivastava, M., Wu, D., Yu, J. Z., and Ying, Q.: New formation and fate of Isoprene SOA markers revealed by field data-constrained modeling, npj Clim Atmos Sci, 6, 1–8, https://doi.org/10.1038/s41612-023-00394-3, 2023.

Zhang, J., Shrivastava, M., Ma, L., Jiang, W., Anastasio, C., Zhang, Q., and Zelenyuk, A.: Modeling Novel Aqueous Particle and Cloud Chemistry Processes of Biomass Burning Phenols and Their Potential to Form Secondary Organic Aerosols, Environ. Sci. Technol., 58, 3776–3786, https://doi.org/10.1021/acs.est.3c07762, 2024.

Zhang, T., Claeys, M., Cachier, H., Dong, S., Wang, W., Maenhaut, W., and Liu, X.: Identification and estimation of the biomass burning contribution to Beijing aerosol using levoglucosan as a molecular marker, Atmospheric Environment, 42, 7013–7021, https://doi.org/10.1016/j.atmosenv.2008.04.050, 2008.

Zhang, Y., Huang, J.-P., Henze, D. K., and Seinfeld, J. H.: Role of isoprene in secondary organic aerosol formation on a regional scale, Journal of Geophysical Research: Atmospheres, 112, https://doi.org/10.1029/2007JD008675, 2007.

Zhang, Y., Ren, H., Sun, Y., Cao, F., Chang, Y., Liu, S., Lee, X., Agrios, K., Kawamura, K., Liu, D., Ren, L., Du, W., Wang, Z., Prévôt, A. S. H., Szidat, S., and Fu, P.: High Contribution of Nonfossil Sources to Submicrometer Organic Aerosols in Beijing, China, Environ. Sci. Technol., 51, 7842–7852, https://doi.org/10.1021/acs.est.7b01517, 2017.

Zhang, Y.-L., Li, J., Zhang, G., Zotter, P., Huang, R.-J., Tang, J.-H., Wacker, L., Prévôt, A. S. H., and Szidat, S.: Radiocarbon-Based Source Apportionment of Carbonaceous Aerosols at a Regional Background Site on Hainan Island, South China, Environ. Sci. Technol., 48, 2651–2659, https://doi.org/10.1021/es4050852, 2014b.

Zhang, Y.-L., Huang, R.-J., El Haddad, I., Ho, K.-F., Cao, J.-J., Han, Y., Zotter, P., Bozzetti, C., Daellenbach, K. R., Canonaco, F., Slowik, J. G., Salazar, G., Schwikowski, M., Schnelle-Kreis, J., Abbaszade, G., Zimmermann, R., Baltensperger, U., Prévôt, A. S. H., and Szidat, S.: Fossil vs. non-fossil sources of fine carbonaceous aerosols in four Chinese cities during the extreme winter haze episode of 2013, Atmospheric Chemistry and Physics, 15, 1299–1312, https://doi.org/10.5194/acp-15-1299-2015, 2015.

Zhang, Y.-L., Kawamura, K., Agrios, K., Lee, M., Salazar, G., and Szidat, S.: Fossil and Nonfossil Sources of Organic and Elemental Carbon Aerosols in the Outflow from Northeast China, Environ. Sci. Technol., 50, 6284–6292, https://doi.org/10.1021/acs.est.6b00351, 2016.

Zhang, Y.-L., El-Haddad, I., Huang, R.-J., Ho, K.-F., Cao, J.-J., Han, Y., Zotter, P., Bozzetti, C., Daellenbach, K. R., Slowik, J. G., Salazar, G., Prévôt, A. S. H., and Szidat, S.: Large

contribution of fossil fuel derived secondary organic carbon to water soluble organic aerosols in winter haze in China, Atmospheric Chemistry and Physics, 18, 4005–4017, https://doi.org/10.5194/acp-18-4005-2018, 2018.

Zhu, C., Kawamura, K., and Kunwar, B.: Effect of biomass burning over the western North Pacific Rim: wintertime maxima of anhydrosugars in ambient aerosols from Okinawa, Atmospheric Chemistry and Physics, 15, 1959–1973, https://doi.org/10.5194/acp-15-1959-2015, 2015a.

Zhu, C., Kawamura, K., and Kunwar, B.: Organic tracers of primary biological aerosol particles at subtropical Okinawa Island in the western North Pacific Rim, Journal of Geophysical Research: Atmospheres, 120, 5504–5523, https://doi.org/10.1002/2015JD023611, 2015b.

Table 1. Concentrations of key $PM_{2.5}$ components in aerosol samples collected during winter pollution episodes in urban Nanjing.

$PM_{2.5}$ ($\mu g\ m^{-3}$)	>200				100-200				<100			
Species	mean	std	min	max	mean	std	min	max	mean	std	min	max
EC ($\mu g\ m^{-3}$)	2.67	0.26	2.27	3.08	2.00	0.08	1.93	2.14	1.73	0.31	1.26	2.24
OC ($\mu g\ m^{-3}$)	35.4	4.78	23.8	41.1	23.7	3.86	18.5	28.7	15.3	6.19	8.74	26.7
TC ($\mu g\ m^{-3}$)	38.1	4.85	26.0	43.4	25.7	3.91	20.5	30.7	17.0	6.39	10.2	28.8
WSOC ($\mu g\ m^{-3}$)	14.3	2.62	8.97	18.1	10.2	1.30	8.11	11.4	6.21	1.90	3.84	8.26
WISOC ($\mu g\ m^{-3}$)	21.1	3.68	14.8	25.8	13.5	2.78	10.4	17.5	9.87	4.64	4.55	19.4
OC/EC	13.3	2.08	10.5	17.4	11.8	1.74	9.57	14.4	8.70	2.72	6.00	13.2
WSOC/OC	0.40	0.06	0.31	0.49	0.43	0.03	0.39	0.47	0.35	0.17	nd	0.51
WISOC/OC	0.60	0.06	0.51	0.69	0.57	0.03	0.53	0.61	0.65	0.17	0.49	1.00
14C-WSOC	0.31	0.06	0.25	0.39	0.25	0.02	0.23	0.28	0.24	0.04	0.18	0.29
Inorganic icons ($\mu g\ m^{-3}$)												
F^-	0.08	0.03	0.05	0.12	0.16	0.20	0.06	0.52	0.05	0.02	0.02	0.08
Cl^-	7.00	1.66	3.86	10.2	6.51	1.50	4.26	7.86	5.51	2.62	1.88	10.2
NO_3^-	56.0	4.39	48.7	62.4	33.9	6.50	24.0	40.1	12.7	4.37	5.75	17.7

SO_4^{2-}	30.9	4.42	26.4	38.8	19.1	3.78	13.2	23.8	10.4	3.95	6.59	19.4
NH_4^+	28.0	3.20	20.3	30.9	17.1	3.60	10.8	19.7	8.52	2.35	4.97	11.4
PO_4^{3-}	0.14	0.02	0.11	0.17	0.07	0.03	0.03	0.12	0.02	0.01	0.01	0.03
Na^+	0.73	0.15	0.47	0.98	0.83	0.18	0.59	1.08	0.47	0.16	0.29	0.76
Ca^{2+}	0.73	0.41	0.35	1.58	1.23	0.55	0.76	1.99	0.40	0.16	0.19	0.62
nss-Ca^{2+}	0.70	0.41	0.32	1.55	1.20	0.55	0.73	1.96	0.38	0.16	0.17	0.61
K^+	0.98	0.24	0.72	1.52	1.01	0.34	0.62	1.40	0.65	0.48	0.22	1.69
nss-K^+	0.95	0.24	0.69	1.49	0.98	0.34	0.60	1.36	0.64	0.48	0.21	1.67
Mg^{2+}	0.69	0.37	0.25	1.18	0.24	0.14	0.10	0.42	0.10	0.07	0.03	0.22
Anhydrosugars (ng m^{-3})												
levoglucosan (L)	471	122	284	721	185	28.1	142	219	201	121	59.0	395
galactosan (G)	39.6	19.1	4.84	63.6	73.2	14.8	55.1	94.1	51.0	44.6	6.70	115
mannosan (M)	45.4	21.2	20.8	81.9	14.8	9.73	4.79	30.3	14.0	8.11	6.63	25.4
L/M	11.5	3.21	5.86	16.5	18.3	12.4	4.67	38.0	22.4	12.7	8.88	38.2
M/G	2.86	4.83	0.41	15.6	0.20	0.13	0.07	0.41	0.66	1.20	nd	3.09
L/K^+	0.51	0.19	0.21	0.76	0.20	0.07	0.14	0.29	0.44	0.33	0.06	1.04
Sugar alcohol (ng m^{-3})												

arabitol	30.5	10.3	12.0	44.1	28.8	10.4	16.6	42.1	17.8	13.4	4.59	48.2
mannitol	14.4	6.24	0.47	24.4	14.2	4.12	7.92	18.4	12.9	7.20	2.43	22.0
glycerol	295	151	119	561	1822	1916	376	4062	2348	1334	652	4749
Sugars (ng m^{-3})												
trehalose	851	874	86.5	2970	1057	1112	302	3023	672	521	257	1378
glucose	203	85.1	49.3	377	312	148	193	551	158	56.0	69.8	240
total measured saccharides	1951	896	633	3841	3507	1632	1738	4976	3474	1238	1478	5436
Isoprene SOA tracers (ng m^{-3})												
cis-2-methyl-1,3,4-trihydroxy-1-butene	0.38	0.42	0.02	1.26	0.62	0.17	0.38	0.85	0.36	0.17	0.11	0.68
3-methyl-2,3,4-trihydroxy-1-butene	0.45	0.67	0.03	2.17	0.59	0.24	0.26	0.93	0.64	0.37	0.01	1.07
trans-2-methyl-1,3,4-trihydroxy-1-butene	0.76	0.83	0.03	2.87	0.99	0.53	0.41	1.81	0.74	0.52	0.06	1.55
sum of C5-Alkene triols	1.59	1.83	0.07	6.30	2.20	0.56	1.66	2.91	1.74	0.99	0.18	3.19
2-methylthreitol	0.69	1.16	0.07	3.78	1.52	0.60	0.65	2.26	1.16	0.92	0.03	3.11
2-methylerythitol	1.17	1.55	0.10	4.93	2.30	0.69	1.29	2.97	2.10	1.19	0.41	4.30

sum of 2-methyltetrols	1.86	2.68	0.20	8.71	3.81	1.20	1.94	4.67	3.26	2.09	0.45	7.41
2-methylglyceric acid	2.05	1.86	0.21	5.93	2.56	0.96	1.13	3.52	1.58	1.09	0.35	3.80
sum of isoprene SOA	5.51	6.23	0.56	20.9	8.58	2.52	4.80	11.1	6.58	4.10	0.97	14.4
Monoterpene SOA tracers (ng m^{-3})												
3HGA	2.45	1.64	0.94	5.52	2.75	2.30	1.02	6.60	0.95	0.39	0.42	1.53
pinonic	1.61	2.15	0.05	6.91	3.41	1.67	1.65	5.64	1.04	0.57	0.38	1.81
pinic	0.32	0.31	0.05	1.06	0.87	0.62	0.24	1.81	0.84	0.69	0.04	1.69
sum of monoterpene SOA	4.38	4.00	1.17	13.5	7.03	3.79	3.22	12.7	2.82	0.90	1.36	4.09
Sesquiterpene SOA tracers (ng m^{-3})												
β-caryophylinic acid	0.26	0.38	nd	1.03	0.22	0.42	nd	0.97	0.29	0.45	nd	1.33
total measured biogenic SOA tracers	10.2	10.2	1.80	34.7	15.8	5.75	8.14	24.3	9.69	4.92	2.36	18.6
Aromatic acids (ng m^{-3})												
phthalic acid (Ph)	8.02	3.05	3.00	12.4	10.5	1.77	8.09	12.8	5.88	3.73	1.45	13.0
isophthalic acid (iPh)	10.1	5.28	0.98	21.2	11.7	6.50	6.75	20.2	5.76	3.32	1.72	11.2
benzoic acid	5.46	2.76	0.47	11.4	5.88	0.52	5.01	6.29	4.47	2.44	1.07	8.41
sum of aromatic acids	23.6	10.2	8.30	45.1	28.1	8.24	21.1	39.3	16.1	8.86	4.25	30.3

Hydroxyl- and polyacids (ng m^{-3})												
glyceric acid	2.20	1.81	0.22	6.56	3.52	1.34	2.00	4.89	2.68	1.48	0.60	5.17
malic acid	3.00	1.45	0.95	5.73	4.32	2.06	1.52	6.60	3.67	1.88	0.77	6.51
tartaric acid	0.45	0.54	0.06	1.89	1.10	0.42	0.49	1.48	1.37	0.83	0.14	2.83
sum of hydroxyl and polyacids	5.66	2.63	1.24	10.4	8.94	3.73	4.01	12.2	7.73	4.14	1.51	14.5
Lignin and resin acids (ng m^{-3})												
4HBA, 4-hydroxybenzoic acid	2.10	2.89	0.36	9.32	2.50	0.86	1.09	3.31	3.40	2.26	0.05	6.02
vanillic acid	1.12	2.05	0.00	5.96	2.50	0.98	1.23	3.53	4.76	3.36	0.02	8.98
syringic acid	28.0	40.7	0.23	97.8	0.21	0.20	0.01	0.54	1.18	2.95	0.01	8.47
dehydroabietic acid	15.3	4.80	4.30	22.7	14.4	7.91	8.22	23.4	17.0	14.0	5.45	40.9
sum of lignin and resin acids	46.5	38.0	15.8	114	19.7	8.78	10.8	29.5	26.3	15.6	9.58	56.1

Note that: OC=organic carbon; TC=total carbon; WSOC=water-soluble OC; WISOC=water-insoluble OC. Water-insoluble OC (WISOC) was calculated as the difference between OC and WSOC. nss-Ca^{2+} refers to non-sea-salt Ca^{2+}. nd: not detected.

Table 2. Concentrations of OC from primary sources (biomass burning, fungal spores, and plant debris) and SOC derived from biogenic and anthropogenic VOCs, along with their contributions to OC in $PM_{2.5}$.

$PM_{2.5}$ concentration (μg m^{-3})	**>200**				**100-200**				**<100**			
	mean	std	min	max	mean	std	min	max	mean	std	min	max
Concentration (μg m^{-3})												
biomass burning-OC	5.79	1.50	3.48	8.86	2.27	0.34	1.74	2.69	2.47	1.48	0.72	4.86
fungal spores-OC	0.44	0.14	0.21	0.62	0.42	0.09	0.32	0.52	0.29	0.18	0.09	0.68
plant debris-OC	0.29	0.12	0.07	0.55	0.45	0.21	0.28	0.80	0.23	0.08	0.10	0.35
sum of primary OC	6.52	1.62	3.77	9.65	3.14	0.46	2.48	3.67	2.99	1.56	1.23	5.39
isoprene SOC	0.03	0.03	0.003	0.09	0.04	0.01	0.02	0.05	0.03	0.02	0.01	0.07
monoterpene SOC	0.02	0.02	0.01	0.06	0.03	0.02	0.01	0.06	0.01	0.004	0.01	0.02
sesquiterpene SOC	0.01	0.02	0.00	0.04	0.01	0.02	0.00	0.04	0.01	0.02	0.00	0.06
sum of biogenic SOC	0.06	0.05	0.01	0.16	0.08	0.04	0.04	0.15	0.06	0.03	0.01	0.10
naphthalene SOC	0.21	0.08	0.08	0.32	0.27	0.05	0.21	0.33	0.15	0.10	0.04	0.34
sum of SOC	0.26	0.11	0.09	0.49	0.36	0.07	0.28	0.44	0.21	0.12	0.05	0.41
total	6.79	1.68	3.86	9.98	3.50	0.50	2.76	4.07	3.20	1.57	1.54	5.62
Contribution to OC (%)												

biomass burning-OC	16.3	3.39	10.6	23.6	9.63	0.56	8.96	10.3	15.9	7.01	8.29	26.5
fungal spores-OC	1.23	0.31	0.74	1.63	1.81	0.47	1.23	2.32	2.38	2.26	0.56	7.50
plant debris-OC	0.83	0.39	0.30	1.74	1.99	1.02	0.98	3.48	1.69	0.75	0.62	2.44
sum of primary OC	18.4	3.62	12.2	25.7	13.4	1.97	11.3	16.0	19.9	8.31	11.5	31.3
isoprene SOC	0.07	0.08	0.01	0.25	0.18	0.08	0.07	0.24	0.23	0.18	0.04	0.60
monoterpene SOC	0.05	0.04	0.02	0.15	0.13	0.08	0.05	0.25	0.09	0.04	0.04	0.15
sesquiterpene SOC	0.03	0.05	0.00	0.14	0.04	0.08	0.00	0.19	0.13	0.22	0.00	0.66
sum of biogenic SOC	0.15	0.14	0.05	0.43	0.36	0.20	0.14	0.67	0.44	0.34	0.09	1.10
naphthalene SOC	0.59	0.21	0.27	0.88	1.17	0.22	0.88	1.46	1.12	0.84	0.29	2.46
sum of SOC	0.74	0.29	0.38	1.28	1.53	0.37	1.01	1.99	1.57	1.13	0.38	3.56
total	19.1	3.74	12.8	26.6	15.0	2.28	12.6	17.8	21.5	8.29	11.9	32.2

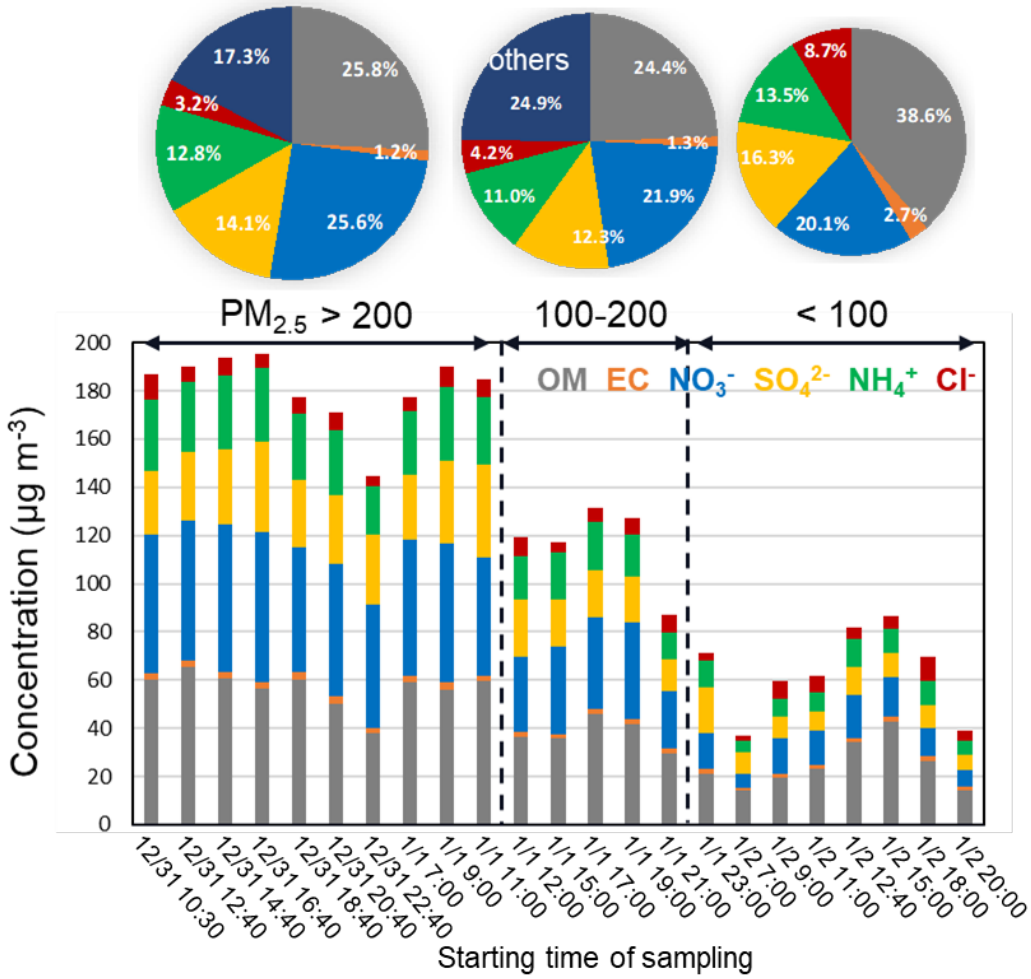

Figure 1. Temporal variations of dominant $PM_{2.5}$ compositions based on different $PM_{2.5}$ levels (<100, 100-200, and >200 μg m^{-3}). Organic matter (OM) concentrations were calculated by multiplying OC concentration by a recommended factor of 1.6 (Turpin and Lim, 2001). "Others" refers to the remaining components of fine particles after removal of organics, secondary inorganic aerosol (sulfate, nitrate, ammonium), and chloride. The pie charts illustrate the average contribution of major components to $PM_{2.5}$ during three pollution episodes.

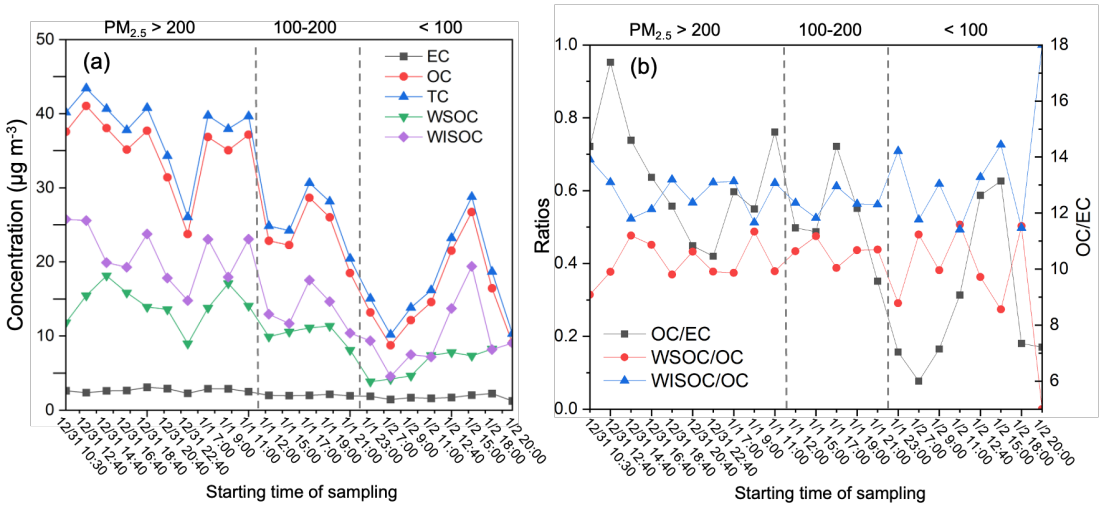

Figure 2. (a) Temporal variations of OC (organic carbon), EC (elemental carbon), WSOC (water-soluble organic carbon), WISOC (water-insoluble organic carbon), TC (total carbon) (units: μg m^{-3}); (b) Ratios of OC/EC, WSOC/OC, and WISOC/OC in $PM_{2.5}$ samples in Nanjing.

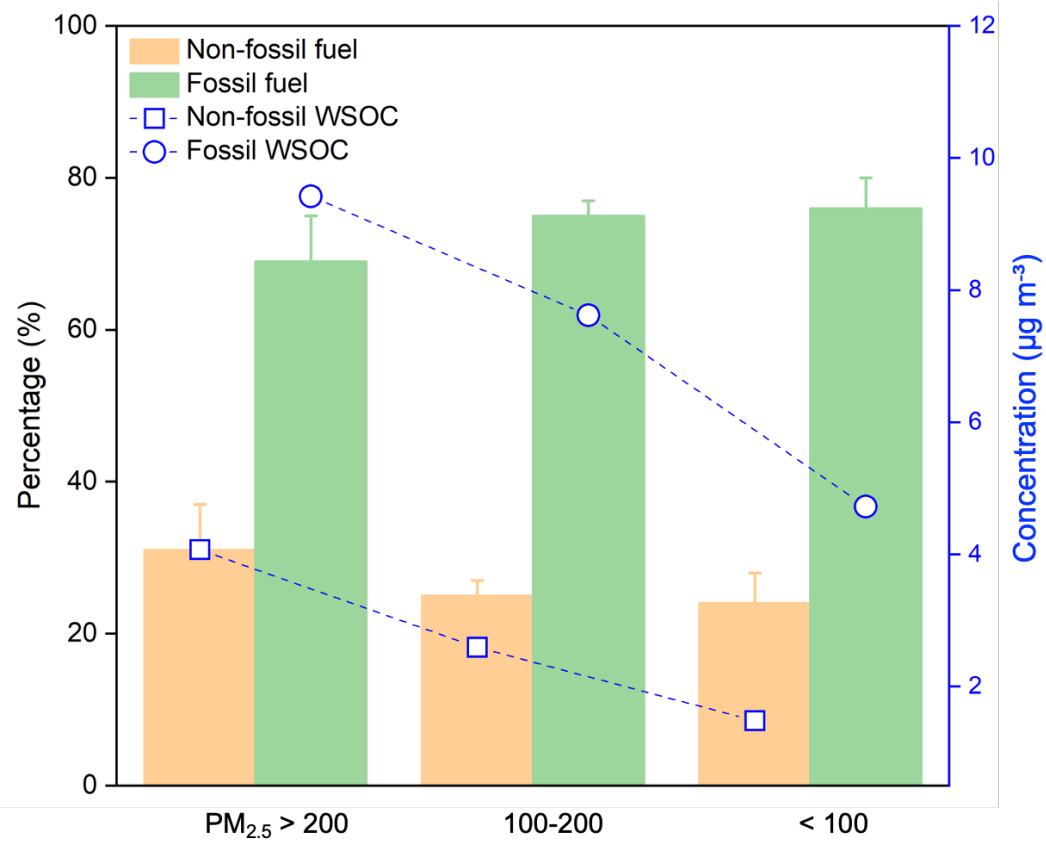

Figure 3. Comparison of fossil and non-fossil contributions to water-soluble organic carbon (WSOC) in urban $PM_{2.5}$ samples during three haze episodes (i.e., $PM_{2.5}$ > 200, 100-200, and < 100 μg m^{-3}).

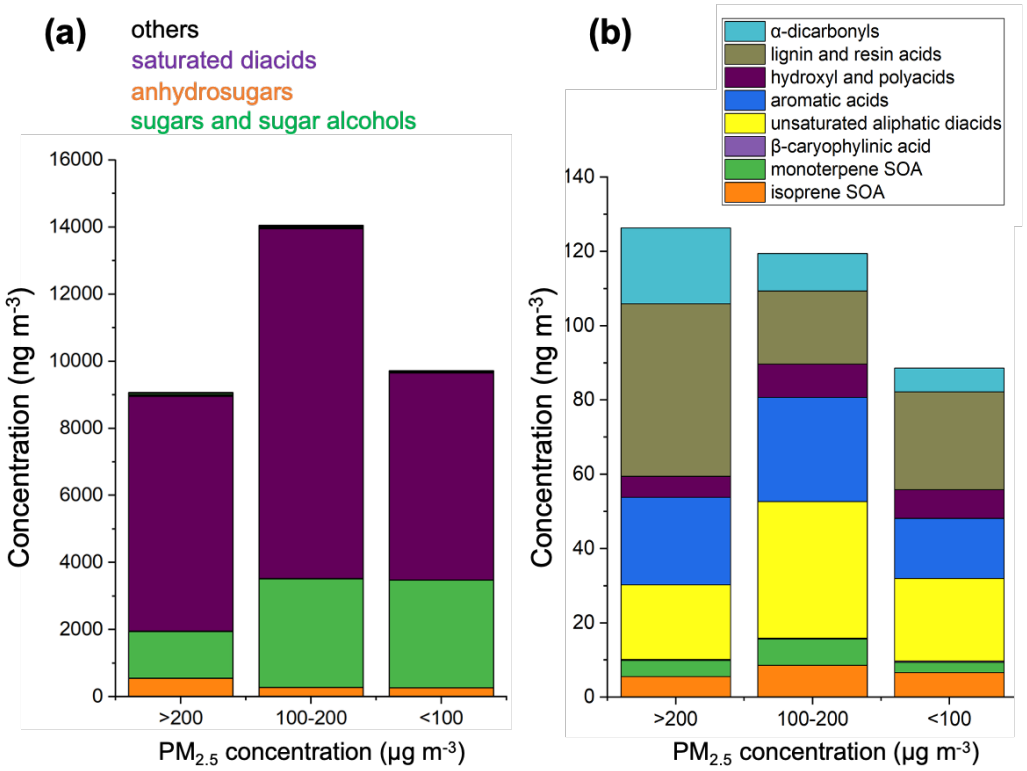

Figure 4. Average concentrations of measured carbonaceous species during three episodes with $PM_{2.5}$ levels of > 200 μg m^{-3}, 100-200 μg m^{-3}, and < 100 μg m^{-3}, respectively. "others" in (a) refers to the total of the components shown in (b).

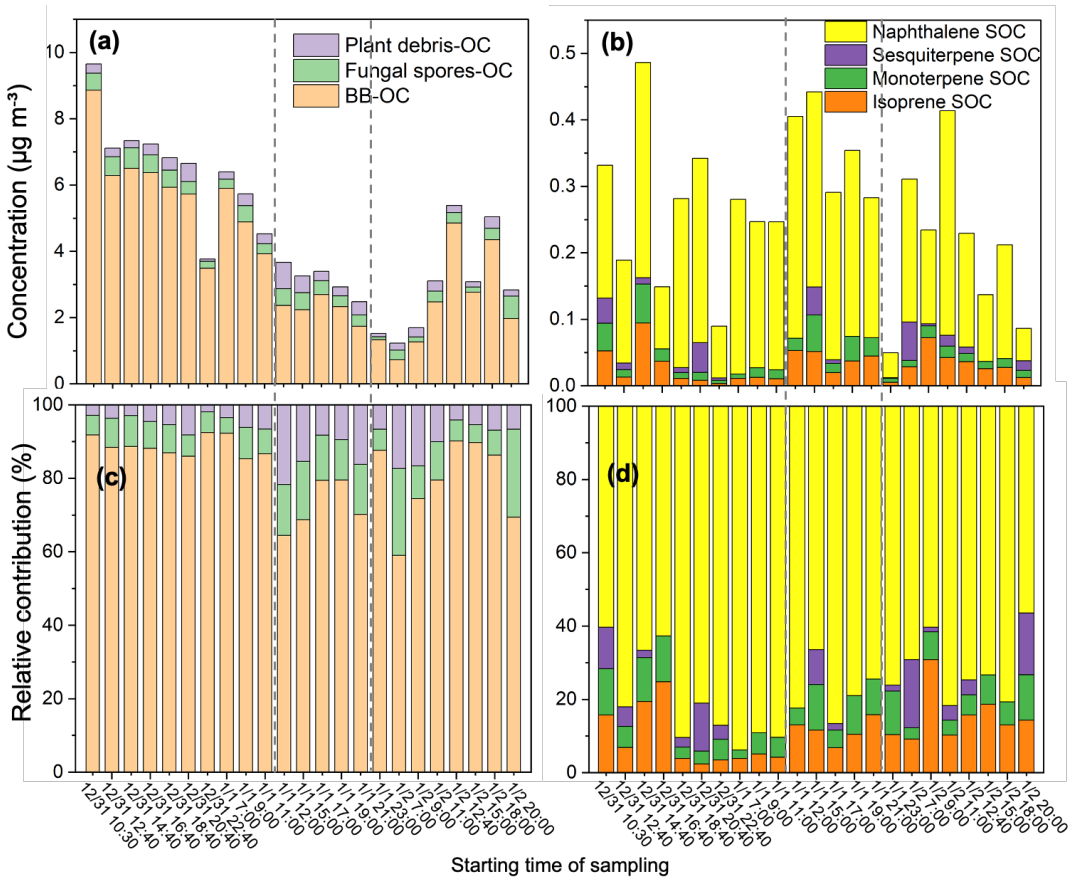

Figure 5. Concentrations of (a) primary OC derived from biomass burning, fungal spores, and plant debris, and (b) secondary OC produced from isoprene, monoterpene, sesquiterpene, and naphthalene, along with their relative contributions (c and d).

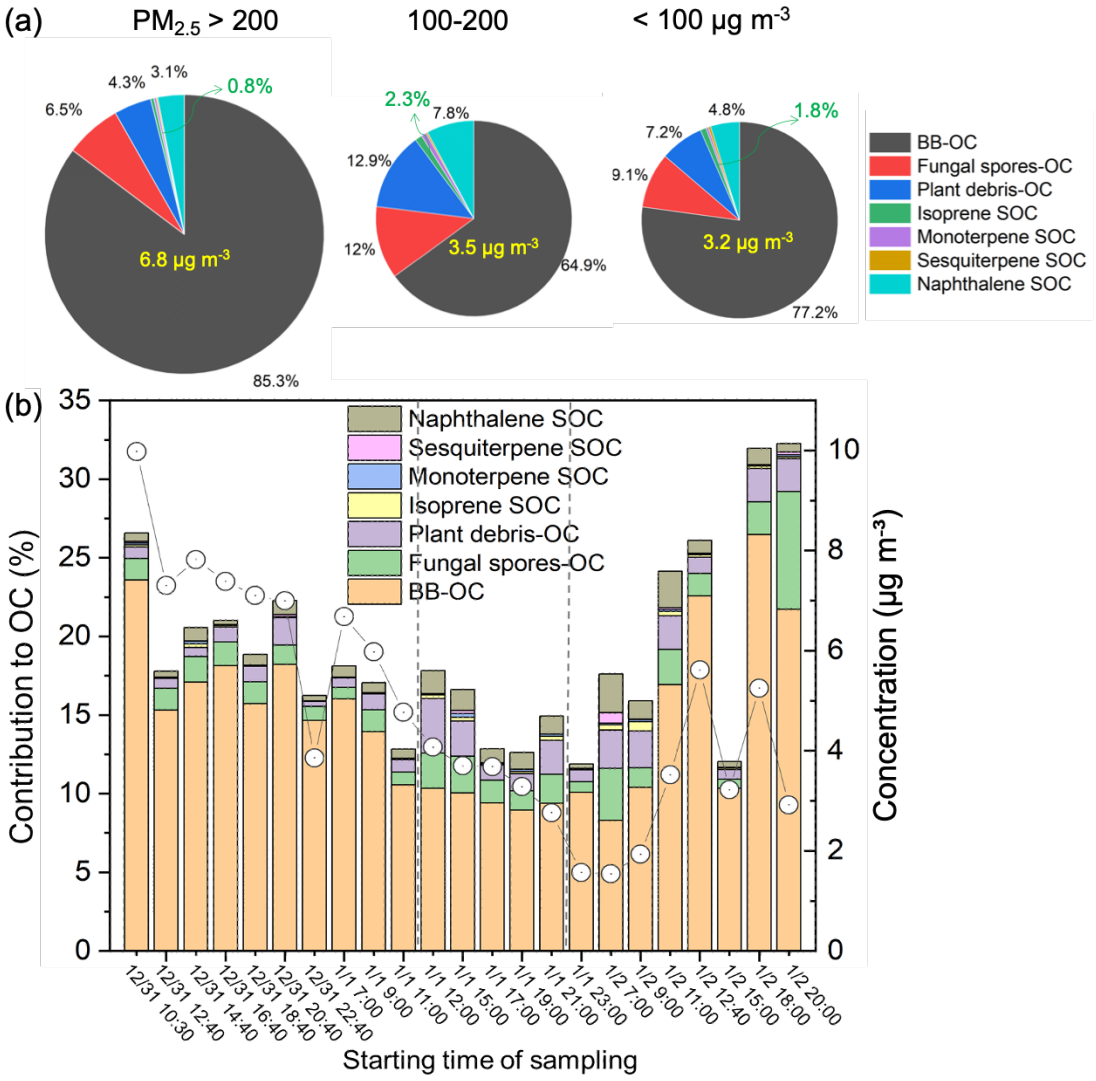

Figure 6. (a) Episode-averaged relative contributions of primary and secondary OC (%). The yellow numbers refer to the total tracer-based OC concentrations attributed to these sources (μg m^{-3}). The size of each pie chart is proportional to its total tracer-based OC concentration. Green arrows and numbers represent the biogenic SOC fraction contributed by isoprene, monoterpene, and sesquiterpene. (b) Contributions of primary and secondary OC to total OC in $PM_{2.5}$ (%), along with OC concentrations attributed to these sources (μg m^{-3}, shown as white circles).